Biogeosciences Discuss., https://doi.org/10.5194/bg-2018-403
Manuscript under review for journal Biogeosciences
Discussion started: 8 October 2018

Distribution, seasonality, optical characteristics, and fluxes of dissolved organic matter (DOM) in the Pearl River (Zhujiang) estuary, China

Yang Li[1], Guisheng Song[2], Philippe Massicotte[3], Fangming Yang[2], Ruihuan Li[4], Huixiang Xie[5,1]

[1] College of Marine and Environmental Sciences, Tianjin University of Science & Technology, Tianjin, 300457, China

[2] School of Marine Science and Technology, Tianjin University, Tianjin, 300072, China

[3] Takuvik Joint International Laboratory (UMI 3376) Université Laval (Canada) & Centre National de la Recherche Scientifique (France), Université Laval, Québec, G1V 0A6, Canada

[4] State Key Laboratory of Tropical Oceanography, South China Sea Institute of Oceanology, Chinese Academy of Science, Guangzhou, 510301, China

[5] Institut des sciences de la mer de Rimouski, Université du Québec à Rimouski, Rimouski (Québec), G5L 3A1, Canada

Correspondence to: Guisheng Song (guisheng.song@tju.edu.cn); Huixiang Xie (huixiang_xie@uqar.ca)

Abstract

Dissolved organic carbon concentration in the Pearl River estuary (PRE) of China was measured in May, August, and October 2015 and January 2016. Chromophoric and fluorescent dissolved organic matter (CDOM and FDOM) in the latter three seasons were characterized by absorption and fluorescence spectroscopy. Parallel factor analysis of the fluorescence spectra identified two protein-like, two humic-like, and one oxidized quinone-like FDOM components. The seasonality of average DOM abundance varied as follows: DOC: May (156 μmol L^{-1}) > January (114 μmol L^{-1}) ≈ August (112 μmol L^{-1}) > November (86 μmol L^{-1}); CDOM absorption at 330 nm: August (1.76 m^{-1}) > November (1.39 m^{-1}) ≈ January (1.30 m^{-1}); FDOM expressed as the sum of the maximum fluorescence intensities of all FDOM components: November (1.77 R.U.) > August (1.54 R.U.) ≈ January (1.49 R.U.). Average DOM abundance in surface water was higher than in bottom water, their difference being marginal (0.1–10%) for DOC in all seasons and for CDOM and FDOM in November and January, and moderate (16–21%) for CDOM and FDOM in August. DOC showed little cross-estuary variations in all seasons while CDOM and FDOM in January were higher on the west side of the estuary than in the middle and on the east side. All three variables exhibited large variations and/or rapid drawdowns at the head of the estuary (salinity <5) due to multiple freshwater endmembers and/or biotic losses. In the saltier zone, they declined linearly with salinity except relatively constant DOC in May and November. The decrease in FDOM was 5–35% faster than that in CDOM, which in turn was 2–3 times faster than that in DOC. Salinity and CDOM absorption coefficients can serve as indicators of DOC in August and January. Absorbance- and fluorescence-based indices demonstrate that freshwater endmembers in all seasons mainly contained fresh, protein-rich DOM of microbial origin, though the proportion of humic-like components was somewhat higher in August. Protein-like materials were preferentially consumed in the low-salinity section but the dominance of the microbial signature was maintained throughout the saltier zone. Exports of DOC and CDOM (in terms of a_{330})

Biogeosciences Discuss., https://doi.org/10.5194/bg-2018-403
Manuscript under review for journal Biogeosciences
Discussion started: 8 October 2018

into the South China Sea were estimated as 195 × 10^9 g and 266 × 10^9 m^2 for the PRE, and 362 × 10^9 g and 493 × 10^9 m^2 for the entire Pearl River Delta. Compared to other world major estuaries, the PRE presents the lowest concentrations and export fluxes of DOC and CDOM. Nonetheless, DOM delivered by the PRE is protein-rich and thus may significantly impact the local ecosystem.

1 Introduction

1.1 Overview of DOM

Dissolved organic matter (DOM) in the ocean drives major biogeochemical cycles involving carbon, nutrients, trace metals, and trace gases (Miller and Zepp, 1995; Cauwet, 2002; Wells, 2002; Cobble, 2007). The chromophoric component of DOM (CDOM), which absorbs solar ultraviolet (UV) and visible radiation (Blough et al., 1993; Nelson et al., 1998; Siegel et al., 2002), affects ocean optics and generates various photoreactions (Mopper and Kieber, 2002; Zafiriou, 2002; Zepp, 2003). The biogeochemical and optical significance of DOM depends on both its abundance and quality (i.e. chemical composition), with the latter strongly linked to its origin of formation (Repeta, 2015; Lønborg et al., 2016, Massicotte et al., 2017).

Coastal waters, particularly those impacted by river plumes, contain higher contents of DOM relative to the open ocean. DOM in river water originates from soil leaching (terrigenous DOM, or tDOM) and in situ microbial production. tDOM, enriched with lignin phenols (Opsahl and Benner, 1997), differs substantially from microbial-derived DOM, enriched with proteins and aliphatic hydrocarbons (Martínez-Pérez, et al., 2017; Brogi et al., 2018), in optical property and biological and photochemical lability (Hansen et al., 2016; Sulzberger and Arey, 2016). Consequently, river runoff can profoundly impact coastal ecosystem functioning by increasing the quantity and altering the quality of DOM in coastal waters.

The loads of terrigenous and microbial DOM and their proportions in a river rely on many factors, among which precipitation and the vegetation type of the catchment area are key players. Forest-covered soils leach tDOM, while agricultural land boosts microbial DOM production by delivering to rivers fertilizers that fuel biological activity. High precipitation during wet seasons flushes more tDOM from soils into rivers compared to low precipitation during dry seasons (Fichot et al., 2014; Li et al., 2015). On the other hand, the residence time of river water during wet seasons is shorter than that during dry seasons, which may decrease autochthonous DOM production (Taylor et al., 2003). Furthermore, DOM in rivers may be subject to physical (e.g. flocculation and coagulation, Asmala et al., 2014), biological (e.g. microbial uptake, Benner and Kaiser, 2011), and chemical (e.g. photobleaching, Vecchio and Blough, 2002) removals during estuarine mixing, thereby reducing its abundance and modifying its chemical and optical properties before being exported to coastal seas. Conversely, biological production can add organic matter to the DOM pool transported downstream from the rivers (Bianchi et al., 2004; Fellman et al., 2010; Benner and Kaiser, 2011; Deutsch et al., 2012). In highly urbanized areas, industrial and residential sewages can be a significant contributor of DOM to river systems (Baker, 2001; Guo et al., 2014). Pollutions not only directly bring in anthropogenic DOM but also carry nutrients that enhance biological DOM production.

1.2 The Pear River estuary

The Pearl River extends for 2214 km and has a catchment area of 450,000 km^2 (Lloyd et al., 2003; Zhang et al., 2008), with its entire drainage basin located south of 27°N in the subtropical zone. After entering the delta area, the Pearl River becomes a complex water network because of the continuous bifurcation of three main tributaries (the West, North, and East Rivers) and other smaller rivers (Fig. 1). The Pearl River system is connected to the South China Sea via three estuaries, Lingdingyang, Modaomen, and Huangmaohai. The Lingdingyang estuary, the principal estuary of the Pearl River, is commonly referred to as the Pearl River estuary (PRE).

The PRE stretches for ~70 km, covers an area of ~2000 km^2, and has an average depth of 4.8 m (Dong et al., 2004). Its topography is featured by three shoals (the east, west, and middle shoals; depths < 2 m) separated by two channels (the east and west channels; depths >5 m) which merge in the upper reach of the estuary near Humen (Wai et al., 2004) (Fig. 1). Tides in the PRE are irregular and semi-diurnal; the mean tidal range is 0.86–1.7 m, increasing landward and reaching >3 m at Humen (Zhao, 1990).

Ranked the second largest in China and the thirteenth largest in the world (Zhang et al., 2008), the Pearl River discharges a freshwater volume of 285 ×10^9 m^3 year^{-1} to the South China Sea. The West River is the largest tributary, contributing 73% of the Pearl River's total freshwater discharge, followed by the North River (14%), and the East River (8%) (Wei and Wu, 2014). The PRE receives 50–55% of the Pearl River's total freshwater flow from four major water outlets, namely Humen, Jiaomen, Hongqimen, and Hengmen (Mikhailov et al., 2006), with Humen providing 35% of the freshwater input to the PRE, followed by Jiaomen (33%), Hengmen (20%), and Hongqimen (12%) (Kot and Hu, 1995). About 70% to 80% of the freshwater discharge in the Pearl River occurs in the wet season (April–September) and only 20–30% in the dry season (October–March) (Wei and Wu, 2014).

Freshwater in the PRE tends to flow seaward along the west side, while coastal saline water intrudes landward along the east channel, causing large cross-estuary salinity gradients (Dong et al., 2004). Seawater intrusion can reach 20–25 km downstream of Humen in the wet season and beyond Humen in the dry season. The water column is strongly stratified during the wet season due to the large freshwater input but well-mixed or far less stratified during the dry season (Wai et al., 2004; Ou et al., 2009).

The Pearl River delivers 30.64 × 10^6 tons of sediment per year into the PRE, with 92–96% of this discharge taking place during the wet season (Xu et al., 1985; Wai et al., 2004). The suspended sediment concentration ranges from 40–300 mg L^{-1} in the wet season and 20–190 mg L^{-1} in the dry season and reaches >100 mg L^{-1} in turbidity maxima occurring at several locations of the estuary (Xu, 1985; Zhao, 1990; Wai et al., 2004).

Phytoplankton biomass in the PRE is generally higher in the wet season than in the dry season but lower than expected from the high concentrations of dissolved inorganic nitrogen (Yin et al., 2000; Harrison et al., 2008; Lu and Gan, 2015; Li et al., 2017). Phytoplankton blooms develop only on local scales, usually in the mid-estuary during the dry season and in the lower part of the estuary during the wet season (Lu and Gan, 2015).

Mountainous and hilly landscapes dominate the drainage basin of the Pearl River with almost no forest (Luo et al., 2002), leading to relatively low dissolved organic carbon concentrations ([DOC]) (117–132 μmol L^{-1}) upstream of the Pearl River Delta (Shi et al., 2016). On the other hand, the Pearl River Delta, a highly urbanized and industrialized region, delivers 5.8×10^9 tons of industrial and domestic sewage per year into the PRE (Lu et al., 2009), which is considered the principal source of DOC in the upper reach of the PRE (Lin, 2007; He, 2010). A number of studies have determined [DOC] and the abundance of CDOM ([CDOM]) (in terms of fluorescence or absorption coefficients) in the PRE (e.g. Dai et al., 2000; Callahan et al., 2004; Chen et al., 2004; Hong et al., 2005; He, 2010; Lei et al., 2018). These studies show no consistent seasonality and estuarine mixing behavior of [DOC] and [CDOM] and no correlation between the variables except one occasion for the mid-salinity (5–20) section of the estuary (Callahan et al., 2004).

The lack of seasonality and consistent estuarine mixing behavior of [DOC] and [CDOM] suggests complex processes controlling their transport, production, and loss in the PRE; it could, however, also result in part from the difference in spatiotemporal coverage of the stations sampled by different

Biogeosciences Discuss., https://doi.org/10.5194/bg-2018-403
Manuscript under review for journal Biogeosciences
Discussion started: 8 October 2018

studies. As previous DOC and CDOM data were collected over a span of 12 and 15 years, respectively, the possibility of interannual variability cannot be ruled out. In addition, none of the past DOC studies surveyed all four seasons and many of them chose two different months to represent the wet and dry seasons, though [DOC] and its mixing behavior may change on smaller time scales. The more limited number of CDOM absorption surveys only sampled a single season with no winter visits. Concerning the spatial coverage, some studies differ substantially in the distribution of sampling stations (e.g. Hong et al., 2005 vs. Lei et al., 2018) and many did not cover the upper reach of the estuary (e.g. Chen et al., 2003; Chen et al., 2004; Wang et al., 2014; Lei et al., 2018).

Compared with the quantitative information on DOC and CDOM, much less is known about the seasonality and mixing behavior of their qualitative aspects. He et al. (2010) examined the DOC compositions (monosaccharides vs. polysaccharides and dissolved free amino acids vs. dissolved combined amino acids) along a longitudinal salinity-gradient transect in the PRE. Hong et al. (2005) determined the fluorescence excitation-emission matrices (EEMs) on samples collected in the dry season and suspected that CDOM in the PRE bears a microbial signature derived from sewage effluents. Besides, spectral slope coefficient (Hong et al., 2005; Lei et al., 2018) and [DOC]-normalized fluorescence intensity (Callahan et al., 2004) have been sporadically used to assess the quality of CDOM in the PRE. Finally, only a few studies have estimated the DOC export flux from the Pearl River to the South China Sea (Lin, 2007; Ni et al., 2008; He et al., 2010), often with limited seasonal coverage. The estimate made by Lin (2007) is almost two times that by Ni et al. (2008). No estimates of CDOM export are available.

1.3 Hypothesis and objectives

Given the large volume and seasonality of the freshwater discharge of the Pearl River, we hypothesize that DOM in the PRE presents substantial seasonal variability in terms of both abundance and chemical composition and that the PRE is an important source of DOM to global oceans. To test this working hypothesis, the present study sampled the same locations in different seasons within a 12-month period, with the objectives of 1) evaluating the seasonality and estuarine mixing behavior of DOC and CDOM in the PRE both quantitatively and qualitatively; 2) improving the estimate of DOC export to the South China Sea; 3) providing the first assessment of seaward export of CDOM in the PRE based on absorption coefficient measurements. Results from this study further increase our understanding of DOM cycling in human-impacted estuarine waters and their contribution to the DOC and CDOM budgets in coastal oceans.

2 Methods

2.1 Sample collection

The sampling area covered the entire PRE, stretching from ~30 km upstream of Humen to the outer limit of the estuary (Fig. 1). Ten stations (M01–M10) were distributed across the main longitudinal axis of the estuary, together with two shorter along-estuary transects, each having four stations on the east (E01–E04) and west (W01–W04) sides. The coordinates of the stations alongside other sampling information are shown in Table 1. Water samples were collected in duplicate from the surface (~1m) and near the bottom (1–2 m above the seabed) using a 5-L plexiglass sampler between 8–12 May, 7–11 August, 16–19 November 2015 and 10–14 January 2016 for [DOC] measurement and in the last three seasons for CDOM analysis. The samples were filtered through 0.2-μm polyethersulfone (PES) filters (Pall Life Sciences) under low vacuum and the filtrates were transferred into 20 mL (DOC) and 100 mL (CDOM) clear-glass bottles with Teflon-lined screw caps. DOC samples were acidified to pH ~2 with 2 N HCl (Reagent grade, Merck). All samples were stored in the dark at 4°C until being analyzed in a land-based laboratory within two weeks after water collection. Prior to use, the glass filtration apparatus and the sample storage bottles were acid-cleaned and combusted at 450°C for 4 h, and the

PES filters were thoroughly rinsed with Milli-Q water and sample water. Water temperature and salinity were determined with a SBE-25 conductivity-temperature-depth (CTD) profiler.

2.2 Sample analysis

[DOC] was determined in triplicate using a Shimadzu TOC-L_{CPH} analyzer calibrated with potassium hydrogen phthalate. The performance of the analyzer was checked, at intervals of 10 consecutive sample analyses, against Hansell's low carbon ([DOC]: 1–2 μmol L^{-1}) and deep Florida Strait ([DOC]: 41–44 μmol L^{-1}) reference waters. The coefficient of variation on five replicate injections was < 2%.

CDOM absorbance spectra were scanned from 800 nm to 200 nm at 1-nm intervals with a Shimadzu UV-2550 dual beam spectrophotometer fitted with 10-cm quartz cells and referenced to Nanopure water. The samples were allowed to warm up to room temperature in darkness before analysis. A baseline correction was made by subtracting the mean absorbance value over 683–687 nm from all spectral values (Babin et al., 2003). The Napierian absorption coefficient, a_{CDOM} (m^{-1}), was calculated as 2.303 times the absorbance divided by the light pathlength of the cell in meters (0.1 m). The analytical uncertainty of a_{CDOM} measurement was assessed by analyzing six pairs of duplicate samples collected from the August cruise. Average a_{CDOM} at 330 nm (a_{330}) was 2.19 m^{-1} (range: 1.19–4.37 m^{-1}); the average difference in each pair was 0.07 ± 0.05 m^{-1}, or 3.0% ± 1.4%.

Fluorescence excitation-emission-matrices (EEMs) were acquired using a Hitachi F-4600 fluorescence spectrophotometer fitted with a 1-cm quartz cuvette to characterize the FDOM composition (Coble, 1996; Boehme et al., 2004). Again, samples were warmed up to room temperature before analysis. Emission spectra were scanned from 230 nm to 600 nm at 2-nm intervals over excitation wavelengths between 200 nm and 450 nm at 5-nm increments. Raman scattering was removed by subtracting Nanopure water EEMs that were scanned on the same day as those for the samples. The spectral fluorescence intensities were normalized to Raman Units (R.U.) following the

Raman Scatter Peak correction reported by Lawaetz and Stedmon (2009). Potential inner-filtering effects were corrected using the obtained absorbance spectra (Ohno, 2002), even though self-shading should be insignificant since the absorption coefficient at 254 nm (a_{254}) was less than 15 m^{-1} for all samples. Major peaks in the EEMs were identified according to the peak definitions proposed in Coble (2007).

PARAFAC analysis was performed to decompose the EEMs into a set of underlying fluorescent components (Bro, 1997; Stedmon et al., 2003; Stedmon and Bro, 2008). The analysis was fed with 117 EEMs from all three seasons sampled for CDOM (Sect. 2.1). To reduce the dominance of high fluorescence intensity signals, the EEMs were first scaled to a unit of variance within the sample mode to construct the calibration model (Bro, 1997). PARAFAC models from 2 to 7 components with constraints of non-negativity in all modes were successively conducted with MATLAB (version 2008b; MathWorks 2008) using DOM Fluorescence Toolbox (DOM Fluor version 1.6) and validated as described by Stedmon and Bro (2008). The parameters obtained from the PARAFAC model were used to calculate an approximate abundance of each component, expressed as F_{max} in Raman's unit (R.U.), which corresponds to the maximum fluorescence intensity for a particular sample. Based on analysis of triplicate samples from Sta. M01, M08, and M10, the uncertainty of F_{max} for each modeled component was <2%.

3 Results

For brevity, seasons and/or water layers for a property are added as a superscript to the symbol or abbreviation denoting that property. For example, $[DOC]^{surf/Aug}$ stands for [DOC] in surface water in August and $a_{330}{}^{btm/Jan}$ for CDOM absorption coefficient at 330 nm in bottom water in January. The slope of linear regression of a property against salinity will be denoted by SLP (Sect. 3.4), with a superscript added to designate the specific variable and/or season. For instance, $SLP^{[DOC]/May}$ denotes the slope of [DOC] vs. salinity in May. [DOM], [CDOM], and [FDOM] stand for the abundances of DOM, CDOM, and FDOM, respectively, and names of PARAFAC components signify their F_{max} as well. Finally, symbols and abbreviations are used as both singular and plural forms.

3.1 Hydrological settings

The average freshwater discharges of the Pearl River for the sampling months were obtained from the Ministry of Water Resources of the P. R. of China (http://www.mwr.gov.cn/zwzc/hygb/sqnb). Assuming that 54% of the total discharge of the Pearl River went into the PRE (Mikhailov et al., 2006) giving 8.9×10^3 m^3 s^{-1} in May, 5.7×10^3 m^3 s^{-1} in August, 6.7×10^3 m^3 s^{-1} in November, and 5.0×10^3 m^3 s^{-1} in January. The freshwater discharge was 15% lower in August than in November due to an atypically dry weather in summer and a relatively higher precipitation in autumn. The precipitation in January was also above average, leading to a higher-than-normal freshwater discharge in that month.

Surface water temperature averaged 27.2°C in May, 30.0°C in August, 25.2°C in November, 18.8°C in January. Water temperature in August was higher in the inner than in the outer estuary, whereas a reverse trend was seen in the other sampling seasons (Fig. S1). Cross-estuary gradients occurred in all four seasons often with irregular patterns. Yet, the east transect showed the highest temperatures in November and the west transect displayed the lowest temperatures in January. The difference between the surface and bottom water was minor in January (0–1.5%) and minor to moderate in May (0–11.9%) and November (0.08–2.5%) except a few stations near the mouth of the estuary. In August, the bottom temperature was substantially lower (3–14%) than the surface temperature at many stations and the difference increased towards the sea.

Surface water salinity (SWS) ranged from 0.2–30.3 (mean: 9.7) in May, 0.2–20.6 (mean: 8.0) in August, 0.2–26.9 (mean: 8.3) in November, and 0.2–32.6 (mean: 17.0) in January. SWS was very low (range: 0.15–0.66) and remained fairly constant upstream of Sta. M05 in May and November (Fig. S2).

Saltwater intruded farther upstream to Sta. M03 in January, in line with the lower tides (Fig. S3) and lower freshwater discharge at that time. Despite August showing the lowest estuary-wide mean SWS among the four seasons, its SWS values in the upper reach of the estuary (Sta. M01–M05) were considerably higher than those in May and November, and the value at Sta. M02 even surpassed that in January. This phenomenon could be partly attributed to most stations in the upper reach being sampled at high tides in August (Fig. S3). Seaward of the upper reach, SWS increased rapidly, albeit with fluctuations likely linked to tidal cycles and passage of salinity fronts (Dong et al., 2004). Consistent with published results (Dong et al., 2004), SWS exhibited cross-estuary gradients, often increasing from the shallow water on the west side to the deeper water on the east side, which was particularly evident in January and May (Fig. S2). Bottom water salinity at most stations was nearly identical to SWS in January, slightly greater in May, moderately elevated in November, and much higher in August (Fig. S2). Based on the salinity difference between the two layers, the water column was mostly well mixed in January, weakly stratified in May, modestly stratified in November, and strongly stratified in August. Remarkable exceptions were certain shallow stations along the west (Sta. W01–W03) and east (Sta. E01) transects at which the water column was well mixed in November and May and weakly stratified in August. In addition, the water column in the low-salinity zone (Sta. W01–W05 in May and November; Sta. W01–W02 in August and January) was essentially homogenous in all four seasons.

3.2 Distributions of quantitative DOM variables

The quantitative DOM variables reported here are [DOC], a_{CDOM}, and PARAFAC-derived FDOM components. a_{330} is chosen as an indicator of [CDOM] (Osburn et al., 2009; Xie et al., 2012; Song et al., 2017). a_{CDOM} at other commonly used wavelengths and the spectral slope coefficient between 300 nm and 500 nm are presented in Table S1. The residual and split-half PARAFAC analyses validated five distinct FDOM components (Fig. 2), which explained 99.75% of the variance and thus adequately modeled the different FDOM profiles in the dataset. Based on published spectral characteristics of PARAFAC-modeled components (e.g. Stedmon et al., 2003; Cory and McKnight, 2005; Yamashita and Jaffé, 2008; Murphy et al., 2008; Santín et al., 2009; Massicotte and Frenette, 2011), components 1 (C1) and 5 (C5) as tyrosine-like and tryptophan-like fluorophores, components 2 (C2) and 4 (C4) were assigned as terrestrial or ubiquitous humic-like DOM fractions, and component 3 (C3) as oxidized quinone-like moieties, respectively. As C1 and C2 are highly correlated with C5 and C4, respectively (Table S2), the sum of C2 and C4 (C2+C4 hereafter) and of C1 and C5 (C1+C5 hereafter) will be used to describe the quantitative distributions of the humic-like and protein-like fractions. C3 is better correlated to C2+C4 (R^2 = 0.953) than to C1+C5 (R^2 = 0.738), suggestive of its humic character.

Table 2 summarizes the ranges and averages of all quantitative variables in different seasons and water layers. The mean $[DOC]^{surf}$ was in descending order of May > January > August > November. The mean a_{330}^{surf}, $(C2+C4)^{surf}$, and $C3^{surf}$ exhibited the same seasonality of August > November > January, differing from that of [DOC]. The seasonal trend of the mean $(C1+C5)^{surf}$ followed November > January > August, inconsistent with the two trends noted above. The seasonality in bottom water was the same as that in surface water for the mean values of all these variables save a_{330} which was equal between November and January in the bottom. The mean values in bottom water were lower than in surface water for all variables and all seasons (Table 2). The seasonal trend of the absolute percent difference between the bottom and surface followed August > May > November > January for [DOC] and August > November > January for the CDOM and FDOM variables, conforming to the successively weakening water column stratification from summer to autumn to winter (Sect. 3.1). The average vertical differences ranged from 6.5–21.0% in August, 1.0–11.9% in November, and 0.1–5.5% in January depending on the variable in question, with [DOC] showing the smallest disparities (Table 2). Despite the overall small vertical gradients, certain stations, often with the deepest water depths (Table 1), did exhibit larger differences (>20%, Fig. S4).

Biogeosciences Discuss., https://doi.org/10.5194/bg-2018-403
Manuscript under review for journal Biogeosciences
Discussion started: 8 October 2018

All variables displayed similar along-estuary distribution patterns characterized by overall declining abundances with increasing seaward distance (Figs. S4,5). Two features are noted here. First, [DOC] in May remained nearly constant from Sta. M01 to M03, consistent with the observation of He et al. (2010) in April 2007. As Sta. M01–M03 all had near-zero salinities (0.18–0.27, Fig. S2) and were distributed across the three entrances of the East River (Fig. 1), freshwater input from this river appeared to have little influence on [DOC] in May. Second, the declines of $[DOC]^{surf}$ across the entire main transect (Fig. 1), 40–42% in May, August, and November, and 54% in January, were considerably lower than those of a_{330} and C1+C5, 70–74% in August, 80–84% in November, and 92–93% in January. The parallel declines of C3 and C2+C4 were somewhat inferior in August (53–57%) but comparable in November (72–76%) and January (92%).

Unlike the substantial cross-estuary salinity gradients noted earlier, lateral variations in [DOC] were generally small in all seasons, with one prominent exception at ~54 km downstream of Sta. M01, where [DOC] in May on the east transect (Sta. E01: 192 μmol L^{-1}) was 47% higher than that on the main transect (Sta. M05: 131 μmol L^{-1}; Fig. S4a). Systematic cross-estuary variations in a_{330} (Fig. S4e–g) and FDOM components (Fig. S5) were not evident in August and November, while values in January were consistently higher along the west transect (Fig. S4g, Fig. S5c,f,i) echoing the substantially lower salinities on the west side (Fig. S2d). Large lateral differences in C1+C5 and C2+C4 were again observed between Sta. E01 on the east transect and Sta. M05 on the main transect in November (Fig. S5b,e).

3.3 Distributions of qualitative DOM metrics

The qualitative metrics reported here are the E_2/E_3 quotient (hereafter E_2/E_3), biological index (BIX), humification index (HIX), and percentages of C1+C5 (%(C1+C5)), C2+C4 (%(C2+C4)), and C3 (%C3) relative to the sum of C1–C5. E_2/E_3, defined as the ratio of a_{250} to a_{365}, serves as a proxy for the average molecular weight (MW) and aromaticity of CDOM, with lower values indicating higher MW and higher aromaticity (Peuravuori and Pihlaja, 1997; Lou and Xie, 2006; Li and Hur, 2017). BIX, the ratio of fluorescence intensity at 380 nm to that at 430 nm with excitation at 310 nm, indicates the relative contribution of fresh, autochthonous FDOM; higher BIX values signify higher contributions of freshly produced FDOM of microbial origin (Huguet et al., 2009). HIX, the ratio of the fluorescence intensity integrated over 435–480 nm to that over 300–345 nm with excitation at 254 nm, is a surrogate of the extent of FDOM humification, with higher values denoting higher degrees of humification (Ohno, 2002). %(C1+C5), %(C2+C4), and %C3 represent the relative contents of protein-like, humic-like, and quinone-like components in the total FDOM pool.

Table 3 summarizes the ranges and averages of all qualitative metrics for each sampling season and water layer. Bottom–surface differences were minor in all seasons and for all metrics. C1+C5 on average accounted for 50.2–66.4% of the total FDOM components and thus exceeded C2+C4 and C3 in all seasons. The seasonal trends of HIX and %(C2+C4) were both August > November > January and opposite to those of E_2/E_3, BIX, and %(C1+C5) (i.e., January > November > August). Note that the difference in E_2/E_3 was marginal between August and November and in all other metrics between November and January. %C3 was highest in August and equal between November and January.

E_2/E_3 in all three seasons increased gradually down-estuary (Fig. S6a–c) by up to 59% in August, 60% in November, and 76% in January. BIX in August and November dropped briefly within the first 10 km and then augmented slowly farther seaward; it remained, however, roughly constant in January (Fig. S6d–f). Mild convex curves with maxima located at mid-estuary characterized the longitudinal HIX distributions in all three seasons (Fig. S6g–i). %(C2+C4) presented an along-estuary distribution pattern (Fig. S7d–f) similar to that of HIX and inverse to that of %(C1+C5) (Fig. S7a–c). With a few exceptions, %C3 increased nearly monotonously from land to sea irrespective of seasons (Fig. S7g–i).

Cross-estuary gradients were generally minor (Figs. S6 and S7). An important exception was the west transect giving lower E_2/E_3 in January, lower %(C1+C5) in August, and higher HIX and

%(C2+C4) in both August and January, with the gradients all diminishing seaward. Bottom–surface differences at individual stations were mostly marginal (<10%). Certain stations, particularly those with relatively deeper water depths (Table 1), showed considerably larger differences (>20%), as noted in Figs. S6 and S7.

3.4 Relationships between quantitative DOM variables and salinity

Surface and bottom data for each variable in each season form a consistent property–salinity pattern (data not shown) and are thus treated as a single dataset. All variables displayed large variations and/or sharp decreases at salinity <5 but remained rather constant ([DOC] in May and November) or declined linearly (all other cases) at salinity >5 (Figs. 3 and 4). Results of linear regressions for the saltier zone are summarized in Table 4. At a 95% confidence level, both the slopes (SLP) and intercepts are statistically no different between August and January for [DOC] and a_{330} and between all three seasons for C3 and C2+C4, indicating that the multi-season data on each of these occasions can be combined into a single dataset. SLP$^{a330/\mathrm{Nov}}$ is, however, ≥32% lower than those in August and January. SLP$^{\mathrm{C1+C5}}$ presents significant seasonal variations, with the value in January 23% and 89% higher than those in November and August, respectively.

The percent decrease of each variable per unit increase of salinity across the saltier zone was calculated using the known regression equations shown in Table 4. a_{330} decreased 2.1 and 2.7 times faster than [DOC] in August and January, respectively (Table S3). [FDOM] declined faster than [CDOM] but their difference was much smaller than that between [CDOM] and [DOC]. The percent decreases in the FDOM components were 5–35% higher than those in a_{330}, with November showing the largest difference (25–35%) followed by August (5–21%) and January (<10%) (Table S3).

3.5 Relationships between qualitative DOM metrics and salinity

Biogeosciences Discuss., https://doi.org/10.5194/bg-2018-403
Manuscript under review for journal Biogeosciences
Discussion started: 8 October 2018

As for the quantitative variables, the surface and bottom data of the qualitative metrics can also be treated as a single dataset in relation to salinity (data not shown). In August and November, E_2/E_3 increased with salinity quickly in the restricted low-salinity section (salinity: <1.3) and slowly in the saltier zone (Fig. 5). In January, the surge at low salinities was less obvious and a gradual rise of E_2/E_3 in the saltier zone was observed up to salinity 28.5 beyond which the trend curved up. All three seasons gave consistent E_2/E_3 vs. salinity patterns from salinity 1.3 to 28.5. In the saltier zone, the data for each season roughly followed the respective theoretical mixing line defined by the maximum- and minimum-salinity E_2/E_3 values in the corresponding season (Fig. 5).

Between salinity 0 and 5, %(C1+C5) in August decreased by approximately 10% (Fig. 6a). In the saltier zone, the west transect displayed an increasing %(C1+C5) with salinity but was constantly below the main and east transects which formed a coherent %(C1+C5) vs. salinity pattern featured by a rebound from salinity 3 to 13 and a continuous decline at salinity >13. In November, %(C1+C5) between salinity 0 and 10 (63.9% ± 5.8%) is more scattered than that for salinity from 10 to 27 (65.1% ± 2.1%) but the average values for the two sections are very similar. %(C1+C5) for the two most marine samples dropped by 5–10% compared with the average over salinity 10–27 (Fig. 6a). A pan shape characterized the distribution of %(C1+C5) in January, revealing higher %(C1+C5) values at both the lowest and highest salinities and relatively lower values across a wide range of salinities in between (Fig. 6a). The distributions of %(C2+C4) vs. salinity approximately mirrored those of %(C1+C5) (Fig. 6b). %C3 in August decreased with salinity along the west transect whereas it increased linearly ($Y = 0.19*X + 15.61$, $R^2 = 0.867$, $n = 28$) along the main and east transects combined (Fig. 6c). %C3 in January stayed rather constant (13.5% ± 0.8%) until an abrupt 14% decline at salinity >32. The distribution of %C3 in November resembled that of %(C2+C4).

Except a few larger scatters at the lowest (November) and highest (November and January) salinities, BIX displayed little dependence on salinity in all three seasons (Fig. 7a). The HIX vs. salinity patterns (Fig. 7b) corresponded to those of %(C2+C4), leading to a strong linear relationship between

Biogeosciences Discuss., https://doi.org/10.5194/bg-2018-403
Manuscript under review for journal Biogeosciences
Discussion started: 8 October 2018

the two variables (Fig. S8a). HIX is also positively correlated to %C3 (Fig. S8b), despite a weaker correlation than that of HIX to %(C2+C4), again suggestive of the humic character of C3 (Sect. 3.2). No significant correlation was seen between BIX and %(C1+C5) (Fig. S8c).

In spite of the certain seasonal and spatial variations of the qualitative metrics noted above, the overall changes of these variables in the saltier zone, after excluding several extreme values for E_2/E_3 and BIX, were fairly limited, ranging from 4.8–9.1, 0.94–1.36, 0.54–2.04, 43.4%–70.3%, 16.5%–35.9%, and 10.4%–22.6% for E_2/E_3, BIX, HIX, %(C1+C5), %(C2+C4), and %C3, respectively.

3.6 Relationships between [DOC] and a_{CDOM} and FDOM fluorescence

[DOC] was linearly correlated to a_{330} for all three sampling seasons; the coefficient of determination was, however, lower in November (Fig. 8a, Table 5). The fitted slope was in descending order of January (32.0 ± 2.0 m μmol L^{-1}) > August (22.5 ± 1.4 m μmol L^{-1}) > November (18.8 ± 2.2 m μmol L^{-1}). Similarly, [DOC] showed a strong, linear correlation with C1+C5 in August and January and a relatively weaker one in November (Fig. 8b, Table 5). The fitted slopes in August and January were comparable but ~2.8 (2.7–2.9) times that in November (Table 5). [DOC] was also significantly related to C2+C4 and C3 (Fig. 8c,d) but the correlations were considerably weaker than that with C1+C5 (Table 5).

4 Discussion

4.1 Sources of freshwater DOM endmembers

Large variations in [DOC] and [CDOM] in the freshwater section of the PRE have been observed previously (Chen et al., 2004; Lin, 2007; He, 2010; Wang et al., 2014; Lei et al., 2018). The present study confirmed this phenomenon in August ([DOC] only) and November ([DOC], [CDOM], and [FDOM]) when near zero-salinity (< 0.7) water was accessible down to Sta. M05 off Hongqimen (Fig. 1). This hefty fluctuation in DOM content is commonly ascribed to the presence of multiple freshwater endmembers delivered by various water channels and outlets described in Sect. 1.2 (Cai et al., 2004; Callahan et al., 2004; He et al., 2010). Because Humen holds most of the sewage discharge from Guangdong Province (Pang and Li, 2001), which carries the highest DOM load, while the other waterways on the west coast, less influenced by urbanization and industrialization, bear lower levels of DOM (Callahan et al., 2004; Ni et al., 2008).

Although the existence of multiple "quantitative" endmembers in the PRE is well recognized, it remains poorly understood if these endmembers differ qualitatively. Data published by Callahan et al. (2004) shows that [DOC]-normalized fluorescences of the freshwater endmembers in Jiaomen, Hongqimen, and Hengmen differed little (c.v. = 4%) while the Humen endmember was 17% higher than the mean of the other three endmembers in November 2002. Besides, fluorescence EEMs collected upstream of Humen reveal tryptophan-like fluorophores to be the dominant FDOM fraction in the Humen endmember which was suspected to originate from sewage effluents (Hong et al., 2005). The present study has analyzed by far the largest number of qualitative metrics (i.e. E_2/E_3, relative abundances of FDOM components, BIX, and HIX) and thus offers a more comprehensive means to assess the nature of the freshwater endmembers. E_2/E_3 in near zero-salinity samples fell in a rather small range from 5.5 to 6.8 that corresponded to a MW range from 0.83 kDa to 1.18 kDa estimated from the MW vs. E_2/E_3 relationship proposed by Lou and Xie (2006). The higher MW values were observed in the Humen channel, while the lower ones in water from Jiaomen and Hongqimen, both being close to the borderline separating the high- and low-MW CDOM (i.e. 1 kDa). %(C1+C5) varied from 70% at Sta. M01 in the Humen channel to 56% off Hongqimen, consistent with a stronger signature of anthropogenic DOC in the Humen channel (He et al., 2010). Yet %(C1+C5) for all endmembers were >50%, demonstrating that protein-like components dominated all freshwater FDOM endmembers. BIX was slightly higher while HIX lower at Sta. M01 than at Sta. M05 (BIX: 1.28 vs. 1.00; HIX: 0.53 vs. 1.34); all BIX and HIX values were, however, well above 0.8 and below 5, respectively, implying the dominance of fresh, microbial-derived FDOM in all freshwater endmembers

(McKnight et al., 2001; Birdwell and Engel, 2010; Sazawa et al., 2011). Taking into account all these qualitative metrics and the linear correlations between [DOC] and the FDOM components (Sect. 3.6), we can conclude that all three freshwater DOM endmembers in November mainly comprised fresh, relatively low-MW (~1 kDa) organic material of microbial origin, with the microbial nature in the Humen endmember somewhat stronger. The sewage influence could be depressed due to a rapid bacterial mineralization of the sewage-derived DOM between the point sources of pollution in the Guangzhou area and the sampling stations downstream (He et al., 2010). Note that the three endmembers also bore a perceptible terrigenous character, since the humic-like C2 and C4, albeit lower in abundance than the protein-like C1 and C5, were still a significant fraction of the total FDOM pool (Fig. 6). The values of the qualitative metrics at Sta. M01 in August and January were comparable to those in November (Figs. S6,7), indicating that the Humen DOM endmembers in summer and winter were also of microbial origin.

Based on an estimate of the relative contributions of land-, sewage-, and phytoplankton-derived DOC, He (2010) and He et al. (2010) proposed that the land component is the dominant source of the total DOC pool in the lower reach of the Humen channel. In this estimation, the authors assigned the "natural background" [DOC] in the three major tributaries of the Pearl River (range: 114–125 μmol L^{-1}; mean: 119 μmol L^{-1}) as "land-derived". Our result suggests that, apart from terrigenous DOC leached from soil, this "land-derived" DOC contains an ample amount of river-born DOC of microbial origin. This is consistent with the poorly forested watershed of the Pearl River (Luo et al., 2002) and with the study of Ni et al. (2008) showing the molar carbon-to-nitrogen ratios of suspended particulate organic matter in all major runoff outlets of the Pearl River Delta (7.2–9.3) to be close to those for phytoplankton and bacterial biomass (5–8).

4.2 Estuarine mixing and transformation of DOM

Biogeosciences Discuss., https://doi.org/10.5194/bg-2018-403
Manuscript under review for journal Biogeosciences
Discussion started: 8 October 2018

Biogeosciences Discussions

Sharp decreases in [DOC], [CDOM], and [FDOM] in the low-salinity section of the PRE have been previously observed and postulated as a result of adsorption, flocculation, biodegradation, and/or incomplete mixing of multiple freshwater endmembers (Callahan et al., 2004; Chen et al., 2004; Lin, 2007; He et al., 2010). The present study confirmed the earlier observations but more importantly provided additional qualitative metrics that are instrumental for constraining the principal processes causing this swift drawdown of [DOM]. The increases in %(C2+C4) and HIX and decreases in %(C1+C5) and BIX in the low-salinity section (Figs. 6 and 7) indicate a bacterial preferential uptake of protein-rich materials and hence a key role of biodegradation in controlling the loss of DOM. Our result corroborates the finding of He et al. (2010) showing higher fractions of biodegradable DOC and higher DOC bio-uptake rates in the low-salinity section than in the saltier zone. Note that the more scattering of the qualitative metrics data in November (Figs. 6 and 7) likely reflects an incomplete mixing of the multiple freshwater endmembers stated earlier. This partial-mixing effect may smear or even entirely overshadow the biodegradation signal.

In the saltier zone, the linear decreases in [DOC] (see exceptions below), [CDOM], and [FDOM] with salinity point to the absence of net removal and input of these constituents and physical dilution being the principal mechanism dictating their estuarine mixing behaviors. The two extreme cases of near-constant [DOC] vs. salinity in May and November indicate that the loss of DOC in the low-salinity section reduced its content to the level comparable to the marine endmember and again that the removal of DOC in the saltier zone, if any, was roughly balanced by the input. Potentially important DOM loss processes in the PRE are bacterial (He et al., 2010) and photochemical (Callahan et al., 2004) degradation. The significance of these processes relies on both their rates and the residence time of freshwater in the PRE. Using the volume of the estuary (9.6×10^9 m^3) and the freshwater discharge rate for each sampling season (Sect. 3.1), we estimated the residence time of freshwater in the top 1-m layer to be 3.1 d in May, 4.9 d in August, 4.1 d in November, and 5.6 d in January. The value for May is essentially identical to that previously reported for the wet season (Yin et al., 2000). Here the volume of the estuary was obtained from the published average depth (4.8 m) and total area (2×10^9 m^2) of the estuary (Dong et al., 2004). The bacterial uptake rate of DOC in surface water of the saltier zone has been reported to be 0.04 μmol L^{-1} h^{-1} in spring and 0.07 μmol L^{-1} h^{-1} in summer, giving a consumption of 3.0 μmol L^{-1} and 8.2 μmol L^{-1}, respectively, when multiplied by the corresponding residence time for May and August. Our unpublished data indicates that photodegradation in August could at most reduce [DOC] by 0.76 μmol L^{-1} and a_{330} by 0.11 m^{-1}, after considering the attenuation of solar radiation and the competition for light absorption by particles in the water column (Wang et al., 2014). The combined photochemical and bacterial DOC degradation in summer was thus ~9 μmol L^{-1}, ~8% of the initial [DOC] in the saltier zone. The parallel photobleaching loss of a_{330} was 7%. Such small losses could be readily compensated for by DOM input from in situ primary production, sediment resuspension, and/or freshwater discharge farther downstream. Notably, chlorophyll *a* concentration maxima of up to 11.0 μg L^{-1} and turbidity maxima of up to 154 mg L^{-1} were spotted in the mid- and lower estuary during our cruises (Xu et al., unpublished data). There was, however, no co-variation of [DOM] (i.e. [DOC], [CDOM], and [FDOM]) with chlorophyll *a* or suspended particle concentration (data not shown). This observation, in conjunction with the linear [DOM] vs. salinity relations, demonstrates that autochthonous production was unlikely a major source of DOM and that adsorption and flocculation were not a major sink of DOM in the saltier zone. The short residence time of freshwater likely minimized the influences of these processes.

The completely different behaviors of [DOC] and [CDOM] with respect to salinity in the saltier zone in November (Fig. 3c,f) led to a decoupling of the two variables. This phenomenon has also been observed for summer by Chen et al. (2004). In fact, the disconnection of [DOC] and [CDOM] is an extreme case of the higher salinity-based [CDOM] gradient relative to that of [DOC] seen in August and January (Sect. 3.4). The difference in estuarine mixing behavior between [DOC] and [CDOM] arose mainly from two factors. First, a large portion of the freshwater DOM endmember was non- and/or weakly colored, as implied by its abundant fresh microbial constituents. Second, the marine endmember's [DOC]-normalized a_{CDOM} was lower than the freshwater endmember's: 0.60 vs. 2.18 L mg^{-1} m^{-1} in August, 0.71 vs. 2.32 L mg^{-1} m^{-1} in November, and 0.26 vs. 1.71 L mg^{-1} m^{-1} in January at 330 nm.

The overall small variations of the qualitative metrics (Figs. 5–7 and Sect. 3.5) across the saltier zone suggest that the chemical composition of CDOM and FDOM remained generally stable during estuarine mixing, consistent with the marginal photochemical and microbial breakdown of DOM elaborated above. The higher values of %(C2+C4), %C3, and HIX in August than in November and January (Figs. 6 and 7) point to FDOM in summer containing a larger fraction of humic-like fluorophores. The divergence in August of the west transect from the main and east transects with respect to the FDOM metrics (save BIX) distributions vs. salinity (Figs. 6 and 7) suggests a different freshwater mass on the west shoal enriched with humic-like FDOM and possibly originating from Hengmen (Fig. 1).

4.3 Indicators of a_{CDOM} and [DOC] in the saltier zone

Salinity is a useful proxy of a_{CDOM} in light of their linear relationships in the saltier zone for all three sampling seasons (Fig. 3). Furthermore, a common equation (Y = −0.048*X + 1.99) can serve as a predictive tool of a_{330} in August and January, given essentially the same statistics for each of these two months (Table 4). For [DOC], salinity can be used as an indicator in August and January but not in May and November (Fig. 3). Similar to the a_{CDOM}–salinity case, the August and January [DOC] data can be combined to formulate a single [DOC]–a_{CDOM} relationship (Y = 40.7*X + 75.6). Hence, [DOC] in summer and winter can in principle be retrieved from remote sensing-based a_{CDOM} data (Siegel et al., 2002; Johannessen et al., 2003; Mannino et al., 2008). Absorption coefficients and fluorescence intensities at the excitation and emission maximum wavelengths of C1 and C5 are also good indicators of [DOC] in August and January (Fig. 8).

Caution should be exercised when applying the [DOC] and a_{CDOM} predictive tools established here, since interannual variability and other factors may limit their applicability on broader time and space scales. For example, Hong et al. (2005) arrived at an a_{CDOM}–salinity relationship of a_{355} = −0.045*salinity + 1.81 for November 2002, which is different from ours in the saltier zone (a_{355} = −0.021*salinity + 0.98). Concurrent measurements of [DOC] and a_{CDOM} in the PRE are rare but Chen et al. (2004) reported no significant correlation between the two variables in July 1999.

4.4 Fluxes of DOC and CDOM

The fluxes of DOC and CDOM exported from the PRE to the South China Sea were estimated as follows (Cai et al., 2004; Lin, 2007; He et al., 2010):

$$F = Q \times C^* \quad (1)$$

where F denotes the flux of DOC or CDOM, Q the freshwater discharge rate, C^* the effective [DOC] ($[DOC]^*$) or a_{330} (a_{330}^*). C^* is the y-axis intercept of the regression line of [DOC] or a_{330} vs. salinity in the saltier zone (Table 4). For May and November when [DOC] remained roughly constant across the saltier zone, C^* signifies the average [DOC] over this zone. Monthly fluxes were computed using freshwater discharge rates for the sampling year and those averaged over 2006–2016 (http://www.mwr.gov.cn/zwzc/hygb/sqnb), under the assumption that the [DOC] or a_{330} obtained for May, August, November, and January represents the entire spring (March, April, May), summer (June, July, August), autumn (September, October, November), and winter (December, January, February), respectively. As no CDOM data was collected in May, the a_{330}^* for spring (1.99 ± 0.19 m^{-1}) was derived from the mean of the $[DOC]^*$-normalized a_{330}^* in January (1.31 L mg^{-1} m^{-1}) and August (1.36 L mg^{-1} m^{-1}) multiplied by the $[DOC]^*$ in May (124.5 μmol L^{-1}). This treatment, with unknown uncertainties, was based on the relatively small variations of the $[DOC]^*$-normalized a_{330}^* among the three CDOM sampling seasons (range: 1.31–1.50 L mg^{-1} m^{-1}).

Biogeosciences Discuss., https://doi.org/10.5194/bg-2018-403
Manuscript under review for journal Biogeosciences
Discussion started: 8 October 2018

Flux estimates for the sampling year are comparable to those for the 10-year period for spring and summer, whereas the former is approximately twice the latter for autumn and winter due to above-average freshwater discharge rates during the low-flow season of the sampling year (Table 6). Aggregation of the fluxes for all four individual seasons arrives at an annual export of 240 × 10^9 g C (sampling year) or 195 × 10^9 g C (10-year period) for DOC and of 329 × 10^9 m^2 (sampling year) or 266 × 10^9 m^2 (10-year period) for CDOM in terms of a_{330}. As the PRE receives ~54% of the total Pearl River freshwater discharge to the South China Sea (Mikhailov et al., 2006), including the rest 46% gives a grand annual export of 362 × 10^9 g C of DOC and 493 × 10^9 m^2 CDOM, respectively, assuming that the fluxes from the PRE are applicable to the entire Pearl River Delta.

4.5 Comparison with previous studies and other major estuaries

The [DOC]s obtained by this study in all four seasons are within the ranges previously reported for the PRE (Table 7). DOC stock in the PRE thus did not seem to undergo large changes over the 7-year span from the last survey in 2008 to our study in 2015, suggesting that the gross inputs and losses of DOM remained stable during this period. Compared to DOC, previous a_{CDOM} measurements are far fewer and none of them was made in wintertime. The summer and autumn a_{330} values from this study are, however, comparable to those published (Table 7). Our DOC flux estimate for spring 2015 (5.8 × 10^8 g C d^{-1}) is close to that reported by He et al. (2010) for spring 2007 (5.3 × 10^8 g C d^{-1}). The summer 2015 value (9.0 × 10^8 g C d^{-1}) is, however, only 60% of the summer 2007's (He, 2010) due to a much lower river runoff in 2015 (7174 m^3 s^{-1} vs. 25060 m^3 s^{-1}). The DOC flux for the entire Pearl River Delta estimated by this study (362 × 10^9 g C $year^{-1}$) is comparable to that (380 × 10^9 g C $year^{-1}$) reported by Ni et al. (2008) but 44% lower than that (650 × 10^9 g C $year^{-1}$) obtained by Lin (2007). The estimate by Ni et al. (2008) was based on monthly [DOC] measurements at eight major runoff outlets of the Pearl River Delta from March 2005 to February 2006. Lin (2007) derived the estimate from data

Biogeosciences Discuss., https://doi.org/10.5194/bg-2018-403
Manuscript under review for journal Biogeosciences
Discussion started: 8 October 2018

collected during three cruises carried out in winter (February 2004), early spring (March 2006), and summer (August 2005). Part of the difference between our study and Lin's could result from the different temporal coverages. The main difference, however, stems from the much greater [DOC]* obtained by Lin (2007) (147 μmol L^{-1} for the wet season and 254 μmol L^{-1} for the dry season).

[DOC] and [CDOM] in the PRE are the lowest among the major world rivers (Table 8). The low DOM load in the PRE could be associated with a deficiency of organic matter in soil of the Pearl River's watershed having almost no forest (Luo et al., 2002). Moreover, although sewage effluents may bring in large amounts of DOM, a big portion of it can be rapidly bio-degraded before reaching the head of the estuary (He et al., 2010). The lack of correspondence between [DOC]* and $a_{330}{}^*$ and the freshwater discharge rate (Fig. S9) suggests that [DOM] in the PRE be controlled by both soil leaching and pollution input. In contrast, DOM in the majority of large rivers is predominantly terrigenous (Bianchi, 2011; Raymond and Spencer, 2015) and the abundance of DOM in many rivers increases with the river flow rate (Cooper et al., 2005; Holmes et al., 2013). Note that the absence of a link between [DOC] and the freshwater discharge rate in the PRE observed by this study differs from the anti-covariation of the two variables reported by Lin (2007) and Ni et al. (2008). Based on this anti-variation, Lin (2007) proposed that the PRE is a typical point source-regulated system in terms of DOC concentration and distribution. It remains to be confirmed if our results imply a fundamental shift of the PRE within ~10 years from a pollution-dominated system to a system jointly controlled by pollution and soil flushing.

Owing mainly to the very low [DOC], our DOC export estimate for the Pearl River is the lowest among the 30 largest rivers worldwide (Raymond and Spencer, 2015), though the Pearl River is ranked the 13th largest river by discharge volume. The Pearl River value of 362×10^9 g C $year^{-1}$ only accounts for 0.14% of the global riverine DOC flux estimate of 250×10^{12} g C $year^{-1}$ (Raymond and Spencer, 2015). The estimate for CDOM export from the Pearl River is also the lowest among the limited

Biogeosciences Discuss., https://doi.org/10.5194/bg-2018-403
Manuscript under review for journal Biogeosciences
Discussion started: 8 October 2018

number of estimates available for the major world rivers (Table 9). It is worth noting that, despite its small contribution on global scales, DOM delivered by the Pearl River is rich in labile, proteinaceous constituents that can be readily utilized by microbes, thereby exerting a potentially important impact on the local ecosystem.

5 Conclusions

The saltier zone of the PRE manifests smaller temporal variabilities and lower spatial gradients of DOM than expected for a sizable estuary with a marked seasonality of river runoff. Several factors functioning in concert lead to this phenomenon. First, a combination of the poorly forested watershed, rapid degradation of pollution-derived DOM in the upper reach, and short residence time of freshwater diminishes [DOM] and seasonal variations in both DOM quantity and quality. Second, the small difference between the low-salinity and marine DOM endmembers tends to lessen the vertical and lateral gradients in DOM again both qualitatively and quantitatively, notwithstanding the larger vertical and cross-estuary salinity gradients. Both the concentrations and seaward exports of DOC and CDOM in and from the PRE are the lowest among the major world rivers. However, as DOM undergoes marginal processing during its transit through the estuary, the Pearl River delivers protein-rich, labile organic matter to the continental shelf of the South China Sea where it may fuel heterotrophy.

Author contributions. GS and HX designed the study. HX and GS interpreted the results and prepared the manuscript with input from PM. YL performed sample analysis and data processing. YL, GS, FY, and RL carried out field sampling. PM conducted PARAFAC modeling.

Competing interests. The authors declare that they have no conflict of interest.

Acknowledgments. We are grateful to the captain and crews of the cruises for their corporation and to Z. Shi, M. Chen, Q. Sun, and L. Han for their help during sampling. Editor's comments improved the manuscript. This study was supported by grants from National Natural Science Foundation of China (41606098 and 41376081) and Tianjin Natural Science Foundation (16JCQNJC08000). HX was holding an adjunct professorship at Tianjin University of Science &Technology during this work.

References:

Asmala, E., Bowers, D. G., Autio, R., Kaartokallio, H., and Thomas, D. N.: Qualitative changes of riverine dissolved organic matter at low salinities due to flocculation, J. Geophys. Res. Biogeosci., 119, 1919–1933, doi:10.1002/2014JG002722, 2014.

Babin, M., Stramski, D., Ferrari, G. M., Claustre, H., Bricaud, A., Obolensky, G., and Hoepffner, N.: Variations in the light absorption coefficients of phytoplankton, nonalgal particles, and dissolved organic matter in coastal waters around Europe, J. Geophys. Res., 108, 3211, doi:10.1029/2001JC000882, 2003.

Baker, A.: Fluorescence excitation-emission matrix characterization of some sewage-impacted rivers, Environ. Sci. Technol., 35, 948–953, 2001.

Benner, R. and Kaiser, K.: Biological and photochemical transformations of amino acids and lignin phenols in riverine dissolved organic matter, Biogeochem., 102, 209–222, 2011.

Bianchi, T. S., Filley, T., Dria, K., and Hatcher, P. G.: Temporal variability in sources of dissolved organic carbon in the lower Mississippi River, Geochim. Cosmochim. Acta, 68, 959–967, 2004.

Bianchi, T. S.: The role of terrestrially derived organic carbon in the coastal ocean: A changing paradigm and the priming effect, P. Nat. Acad. Sci. USA, 108(49), 19473–19481, 2011.

Birdwell, J. E., and Engel, A. S.: Characterization of dissolved organic matter in cave and spring waters using UV-Vis absorbance and fluorescence spectroscopy, Org. Geochem., 41, 270–280, 2010.

Blough, N. V., Zafiriou, O. C., and Bonilla, J.: Optical absorption spectra of waters from the Orinoco River outflow: terrestrial input of colored organic matter to the Caribbean, J. Geophy. Res., 98(2), 2271–2278, doi:10.1029/92JC02763, 1993.

Biogeosciences Discuss., https://doi.org/10.5194/bg-2018-403
Manuscript under review for journal Biogeosciences
Discussion started: 8 October 2018

Boehme, J., Coble, P., Conmy, R., and Stovall-Leonard, A.: Examining CDOM fluorescence variability using principal component analysis: seasonal and regional modeling of three-dimensional fluorescence in the Gulf of Mexico, Mar. Chem., 89, 3–14, 2004.

Bro, R.: PARAFAC. Tutorial and applications, Chemom. Intell. Lab. Syst., 38, 149–171, 1997.

Brogi, S. R., Ha, S.-Y., Kim, K., Derrien, M., Lee, Y. K., and Hur, J.: Optical and molecular characterization of dissolved organic matter (DOM) in the Arctic ice core and the underlying seawater (Cambridge Bay, Canada): Implication for increased autochthonous DOM during ice melting, Sci. Total Environ., 627, 802–811, 2018.

Cai, W., Dai, M., Wang, Y., Zhai, W., Huang, T., Chen, S., Zhang, F., Chen, Z., and Wang, Z.: The biogeochemistry of inorganic carbon and nutrients in the Pearl River estuary and the adjacent Northern South China Sea, Cont. Shelf Res., 24, 1301–1319, 2004.

Callahan, J., Dai, M., Chen, R., Li, X., Lu, Z., and Huang, W.: Distribution of dissolved organic matter in the pearl river estuary, China, Mar. Chem., 89, 211–224, 2004.

Cao, F., Medeiros, P. M., and Miller, W. L.: Optical characterization of dissolved organic matter in the Amazon River plume and the adjacent ocean: examining the relative role of mixing, photochemistry, and microbial alterations, Mar. Chem., 186, 178-188, 2016.

Cauwet, G.: DOM in the coastal zone, in: Biogeochemistry of marine dissolved organic matter, edited by: Hansell, D. A. and Carlson, C. A., Academic Press, San Diego, USA, 579–609, 2002.

Chen, C., Shi, P., Yin, K., Pan, Z., Zhan, H., and Hu, C.: Absorption coefficient of yellow substance in the Pearl River estuary, Proc. of SPIE, 4892, 215–221, 2003.

Chen, Z., Li, Y., and Pan, J.: Distributions of colored dissolved organic matter and dissolved organic carbon in the Pearl River estuary, China, Cont. Shelf Res., 24, 1845–1856, 2004.

Coble, P. G.: Characterization of marine and terrestrial DOM in seawater using excitation-emission matrix spectroscopy, Mar. Chem., 51, 325–346, 1996.

Coble, P. G.: Marine optical biogeochemistry: the chemistry of ocean color, Chem. Rev., 107, 402–418, 2007.

Cooper, L. W., Benner, R., McClelland, J. W., Peterson, B. J., Holmes, R. M., Raymond, P. A., Hansell, D. A., Grebmeier, J. M., and Codispoti, L. A.: Linkages among runoff, dissolved organic carbon and the stable oxygen isotope composition of seawater and other water mass indicators in the Arctic Ocean, J. Geophys. Res., 110, G02023, doi:10.1029/2005JG000031, 2005.

Cory, R. M., and McKnight, D. M.: Fluorescence spectroscopy reveals ubiquitous presence of oxidized and reduced quinones in dissolved organic matter, Environ. Sci. Technol., 39(21), 8142–8149, 2005.

Dai, M., Jean-Marie, M., Hong, H., and Zhang, Z.: Preliminary study on the dissolved and colloidal organic carbon in the Zhujiang river estuary, Chin. J. Oceanol. Limnol., 18(3), 265–273, 2000.

Deutsch, B., Alling, V., Humborg, C., Korth, F., and Mörth, C. M.: Tracing inputs of terrestrial high molecular weight dissolved organic matter within the Baltic Sea ecosystem, Biogeosciences, 9, 4465–4475, 2012.

Dong, L., Su, J., Wong, L., Cao, Z., and Chen, J.: Seasonal variation and dynamics of the Pearl River plume, Cont. Shelf Res., 24, 1761–1777, 2004.

Fellman, J. B., Hood, E., and Spencer, R. G. M.: Fluorescence spectroscopy opens new windows into dissolved organic matter dynamics in freshwater ecosystems: a review, Limnol. Oceanogr., 55, 2452–2462, 2010.

Fichot, C. G., Lohrenz, S. E., and Benner, R.: Pulsed, cross-shelf export of terrigenous dissolved organic carbon to the Gulf of Mexico, J. Geophys. Res. Oceans, 119, doi:10.1002/2013JC009424, 2014.

Guo, W., Yang, L., Zhai, W., Chen, W., Osburn, C. L., Huang, X., and Li, Y.: Runoff-mediated seasonal oscillation in the dynamics of dissolved organic matter in different branches of a large bifurcated estuary-the Changjiang estuary, J. Geophys. Res. Biogeosci., 119, 776–793, 2014.

Hansen, A. M., Kraus, T. E. C., Pellerin, B. A., Fleck, J. A., Downing, B. D., and Bergamaschi, B. A.: Optical properties of dissolved organic matter (DOM): Effects of biological and photolytic degradation, Limnol. Oceanogr., 61(3), 1015–1032, 2016.

Harrison, P. J., Yin, K., Lee, J. H. W., Gan, J., and Liu, H.: Physica-biological coupling in the pearl river estuary, Cont. Shelf Res., 28, 1405–1415, 2008.

He, B., Dai, M., Zhai, W., Wang, L., Wang, K., Chen, J., Lin, J., Hua, A., and Xu, Y.: Distribution, degradation and dynamics of dissolved organic carbon and its major compound classes in the pearl river estuary, China, Mar. Chem., 119, 52–64, 2010.

He, B.: Organic Matter in the Pearl River Estuary: its Composition, Source, Distribution, Bioactivity and their Linkage to Oxygen Depletion (Ph.D. Dissertation), Xiamen university, 2010 (In Chinese).

Holmes, R. M., Coe, M. T., Fiske, G. J., Gurtovaya, T., McClelland, J. W., Shiklomanov, A. I., Spencer, R. G. M., Tank, S. E., Zhulidov, A. V.: Climate change impacts on the hydrology and biogeochemistry of Arctic Rivers, in: Climatic Change and Global Warming of Inland Waters: Impacts and Mitigation for Ecosystems and Societies, edited by: Goldman, C. R., Kumagai, M., and Robarts, R. D., Wiley-Blackwell: Hoboken, NJ, 3−26, 2013

Hong, H., Wu, J., Shang, S., and Hu, C.: Absorption and fluorescence of chromophoric dissolved organic matter in the Pearl River Estuary, South China, Mar. Chem., 97, 78–89, 2005.

Hudon, C., Gagnon, P., Rondeau, M., Hébert, S., Gilbert, D., Hill, B., Patoine, M., and Starr, M.: Hydrological and biological processes modulate carbon, nitrogen and phosphorus flux from the St. Lawrence River to its estuary (Quebec, Canada), Biogeochem., 135, 251–276, 2017.

Huguet, A., Vacher, L., Relexans, S., Saubusse, S., Froidefond, J. M., and Parlanti, E.: Properties of fluorescent dissolved organic matter in the Gironde Estuary, Org. Geochem., 40, 706–719, 2009.

Johannessen, S. C., Miller, W. L., and Cullen J. J.: Calculation of UV attenuation and colored dissolved organic mater absorption spectra from measurements of ocean color, J. Geophys. Res., 108(C9), 3301, doi:10.1029/2000JC000514, 2003.

Kot, S. C. and Hu, S. L.: Water flows and sediment transport in Pearl River Estuary and wave in South China Sea near Hong Kong, coastal infrastructure development in Hong Kong-a review, Hong Kong Government, Hong Kong, 1995.

Lawaetz, A. J. and Stedmon, C. A.: Fluorescence Intensity Calibration Using the Raman Scatter Peak of Water, Appl. Spectrosc., 63, 936–940, 2009.

Lei, X., Pan, J., and Devlin, A. T.: Mixing behavior of chromophoric dissolved organic matter in the Pearl River estuary in spring, Cont. Shelf Res., 154, 46–54, 2018.

Li, P., and Hur, J.: Utilization of UV-Vis spectroscopy and related data analyses for dissolved organic matter (DOM) studies: A review, Crit. Rev. Environ. Sci. Technol., 47(3), 131–154, 2017.

Li, P., Chen, L., Zhang, W., and Huang, Q.: Spatiotemporal distribution, sources, and photobleaching imprint of dissolved organic matter in the Yangtze estuary and its adjacent sea using fluorescence and parallel factor analysis, PLoS ONE, 10, e0130852, doi:10.1371/journal.pone.0130852, 2015.

Li, R., Xu, J., Li, X., and Harrison, P. J.: Spatiotemporal Variability in Phosphorus Species in the Pearl River Estuary: Influence of the River Discharge, Sci. Rep., 7, 13649, doi:10.1038/s41598-017-13924-w, 2017.

Lin, J.: On the behavior and flux of Dissolved Organic Carbon in two large Chinese estuaries-Changjiang and Zhujiang (Master Dissertation), Xiamen university, 2007 (In Chinese).

Lloyd, J. M., Zong, Y., Jung, M., and Yim, W.: Reconstruction of Holocene monsoon variability and sea-level changes from the Pearl River estuary, Geophys. Res. Abs., 5, 02171, 2003.

Lønborg, C., Nieto-Cid, M., Hernando-Morales, V., Hernández-Ruiz, M., Teira, E., and Álvarez-Salgado, X. A.: Photochemical alteration of dissolved organic matter and the subsequent effects on bacterial carbon cycling and diversity, FEMS Microbiol. Ecol., 92, fiw048, doi:10.1093/femsec/fiw048, 2016.

Lou, T., and Xie, H.: Photochemical alteration of the molecular weight of dissolved organic matter, Chemosphere, 65, 2333–2342, 2006.

Biogeosciences Discuss., https://doi.org/10.5194/bg-2018-403
Manuscript under review for journal Biogeosciences
Discussion started: 8 October 2018

Lu, F., Ni, H., Liu, F., and Zeng, E.: Occurrence of nutrients in riverine runoff of the Pearl River Delta, South China, J. Hydrol., 376, 107–115, 2009.

Lu, Z. and Gan, J.: Controls of seasonal variability of phytoplankton blooms in the pearl river estuary, Deep-Sea Res. Part II, 117, 86–96, 2015.

Luo, X. L., Yang, Q. S., and Jia, L. W.: River-bed evolution of the Pearl River Delta network, Sun Yat-sen University Press, Guangzhou, China, p213, 2002 (in Chinese).

Mannino, A., Russ, M. E., and Hooker, S. B.: Algorithm development and validation for satellite-derived distributions of DOC and CDOM in the U.S. Middle Atlantic Bight, J. Geophys. Res., 113, C07051, doi:10.1029/2007JC004493, 2008.

Martínez-Pérez, A. M., Osterholz, H., Nieto-Cid, M., Álvarez, M., Dittmar, T., and Álvarez-Salgado, X. A.: Molecular composition of dissolved organic matter in the Mediterranean Sea, Limnol. Oceanogr., 62, 2699-2712, 2017.

Massicotte, P., and Frenette, J.-J.: Spatial connectivity in a large river system: resolving the sources and fate of dissolved organic matter, Ecol. Appl., 21(7), 2600–2617, 2011.

Massicotte, P., Asmala, E., Stedmon, C., and Markager, S.: Global distribution of dissolved organic matter along the aquatic continuum: Across rivers, lakes and oceans, Sci. Total Environ., 609, 180–191, 2017.

McKnight, D. M., Boyer, E. W., Westerhoff, P. K., Doran, P. T., Kulbe, T., and Andersen, D. T.: Spectrofluorometric characterization of dissolved organic matter for indication of precursor organic material and aromaticity, Limnol. Oceanogr., 46, 38–48, 2001.

Mikhailov, V. N., Mikhailova, M. V., and Korotaev, V. N.: Hydrological and morphological processes at the Zhujiang River mouth area, China, Water Resour., 33, 237–248, 2006.

Miller, W. L. and Zepp, R. G.: Photochemical production of dissolved inorganic carbon from terrestrial organic matter: significance to the oceanic organic carbon cycle, Geophys. Res. Lett., 22, 417–420, 1995.

Mopper, K., and Kieber, D. J.: Photochemistry and the cycling of carbon, sulfur, nitrogen and phosphorus, in: Biogeochemistry of marine dissolved organic matter, edited by: Hansell, D. A. and Carlson, C. A., Academic Press, San Diego, USA, 456–508, 2002.

Murphy, K. R., Stedmon, C. A., Waite, T. D., and Ruiz, G. M.: Distinguishing between terrestrial and autochthonous organic matter sources in marine environments using fluorescence spectroscopy, Mar. Chem., 108, 40–58, 2008.

Nelson, N. B., Siegel, D. A., and Michaels, A. F.: Seasonal dynamics of colored dissolved material in the Sargasso Sea, Deep-Sea Res. Part II, 45, 931–957, 1998.

Ni, H., Lu, F., Luo, X., Tian, H., and Zeng, E.: Riverine inputs of total organic carbon and suspended particulate matter from the Pearl River Delta to the coastal ocean off South China, Mar. Pollut. Bull., 56, 1150–1157, 2008.

Ohno, T.: Fluorescence inner-filtering correction for determining the humification index of dissolved organic matter, Environ. Sci. Technol., 36, 742–746, 2002.

Opsahl S. and Benner R.: Distribution and cycling of terrigenous dissolved organic matter in the ocean, Nature, 386, 480–482, 1997.

Osburn, C. L., Retamal, L., and Vincent, W. F.: Photoreactivity of chromophoric dissolved organic matter transported by the Mackenzie River to the Beaufort Sea, Mar. Chem., 115, 10–20, 2009.

Ou, S., Zhang,H., and Wang, D.: Dynamics of the buoyant plume off the Pearl River Estuary in summer, Environ. Fluid Mech., 9, 471–492, 2009.

Pang, Y., and Li, Y. S.: Effects of discharged pollutants from Pearl River delta on east outlets, J. Hohai Univ., 29(4), 50–55, 2001.

Peuravuori, J., and Pihlaja, K.: Molecular size distribution and spectroscopic properties of aquatic humic substances, Anal. Chim. Acta, 337, 133–149, 1997.

Raymond, P. A., and Spencer, R. G. M.: Riverine DOM, in: Biogeochemistry of marine dissolved organic matter, second edition, edited by: Hansell, D. A. and Carlson, C. A., Academic Press, San Diego, USA, 509–533, 2015.

Raymond, P. A., McClelland, J. W., Holmes, R. M., Zhulidov, A. V., Mull, K., Peterson, B. J., Striegl, R. G., Aiken, G. R., and Gurtovaya, T. Y.: Flux and age of dissolved organic carbon exported to the Arctic Ocean: A carbon isotopic study of the five largest arctic rivers, Global Biogeochem. Cycles, 21, GB4011, doi:10.1029/2007GB002934, 2007.

Repeta, D. J.: Chemical characterization and cycling of dissolved organic matter, in: Biogeochemistry of marine dissolved organic matter, second edition, edited by: Hansell, D. A. and Carlson, C. A., Academic Press, San Diego, USA, 20–63, 2015.

Santín, C., Yamashita, Y., Otero, X. L., Álvarez, M. Á, and Jaffé, R.: Characterizing humic substances from estuarine soils and sediments by excitation-emission matrix spectroscopy and parallel factor analysis, Biogeochem., 96, 131–147, 2009.

Sazawa, K., Tachi, M., Wakimoto, T., Kawakami, T., Hata, N., Taguchi, S., and Kuramitz, H.: The evaluation for alterations of DOM components from upstream to downstream flow of rivers in Toyama (Japan) using three-dimensional excitation-emission matrix fluorescence spectroscopy, Int. J. Environ. Res. Public Health, 8, 1655–1670, 2011.

Biogeosciences Discuss., https://doi.org/10.5194/bg-2018-403
Manuscript under review for journal Biogeosciences
Discussion started: 8 October 2018

Shi., G., Peng., C., Wang, M., Shi, S., Yang, Y., Chu, J., Zhang, J., Lin, G., Shen, Y., and Zhu, Q.: The spatial and temporal distribution of dissolved organic carbon exported from three Chinese rivers to the China sea, PLoS ONE, 11(10), e0165039, doi:10.1371/journal.pone.0165039, 2016.

Seidel, M., Dittmar, T., Ward, N. D., Krusche, A. V., Richey, J. E., Yager, P. L., and Medeiros, P. M.: Seasonal and spatial variability of dissolved organic matter composition in the lower Amazon River, Biogeochem., 131, 281-302, doi:10.1007/s10533-016-0279-4, 2016.

Siegel, D. A., Maritorena, S., Nelson, N. B., Hansell, D. A., and Lorenzi-Kayser, M.: Global distribution and dynamics of colored dissolved and detrital organic materials, J. Geophys. Res., 107, 32–28, 2002.

Song, G., Li, Y., Hu, S., Li, G., Zhao, R., Sun, X., and Xie, H.: Photobleaching of chromophoric dissolved organic matter (CDOM) in the Yangtze River estuary: kinetics and effects of temperature, pH, and salinity, Environ. Sci.: Processes Impacts, 19, 861–873, 2017.

Spencer, R. G. M., Aiken, G. R., Dornblaser, M. M., Butler, K. D., Holmes, R. M., Fiske, G., Mann, P. J., and Stubbins, A.: Chromophoric dissolved organic matter export from U.S. rivers, Geophys. Res. Lett., 40, 1575–1579, doi:10.1029/grl50357, 2013.

Stedmon, C. A. and Bro, R.: Characterizing dissolved organic matter fluorescence with parallel factor analysis: a tutorial, Limnol. Oceanogr. Methods, 6, 1–6, 2008.

Stedmon, C. A., Amon, R. M. W., Rinehart, A. J., and Walker, S. A.: The supply and characteristics of colored dissolved organic matter (CDOM) in the Arctic Ocean: Pan Arcitc trends and differences, Mar. Chem., 124, 108–118, 2011.

Stedmon, C. A., Markager, S., and Bro, R.: Tracing dissolved organic matter in aquatic environments using a new approach to fluorescence spectroscopy, Mar. Chem., 82, 239–254, 2003.

Sulzberger, B. and Arey, J. S.: Impacts of polar changes on the UV-induced mineralization of terrigenous dissolved organic matter, Environ. Sci. Technol., 50, 6621–6631, 2016.

Taylor, G. T., Way, J., and Scranton, M. I.: Planktonic carbon cycling and transport in surface waters of the highly urbanized Hudson River estuary, Limnol. Oceanogr., 48, 1779–1795, 2003.

Vecchio, R. D. and Blough, N. V.: Photobleaching of chromophoric dissolved organic matter in natural waters: kinetics and modeling, Mar. Chem., 78, 231–253, 2002.

Wai, O., Wang, C., Li, Y., and Li, X.: The formation mechanisms of turbidity maximum in the Pearl River estuary, China, Mar. Pollut. Bull., 48, 441–448, 2004.

Wang, S., Wang, Y., Fu, Q., Yin, B., and Li, Y.: Spectral absorption properties of the water constituents in the estuary of Zhujiang River, Environ. Sci., 35, 4511–4521, 2014 (In Chinese).

Wang, X., Ma, H., Li, R., Song, Z., and Wu, J.: Seasonal fluxes and source variation of organic carbon transported by two major Chinese rivers: the Yellow River and Changjiang (Yangtze) River, Global Biogeochem. Cycles, 26, GB2025, doi:10.1029/2011GB004130, 2012.

Wei, X. and Wu, C.: Long-term process-based morphodynamic modeling of the Pearl River Delta, Ocean Dynam., 64, 1753–1765, 2014.

Wells, M. L.: Marine colloids and trace metals, in: Biogeochemistry of marine dissolved organic matter, edited by: Hansell, D. A. and Carlson, C. A., Academic Press, San Diego, 367–404, 2002.

Xie, H., Aubry, C., Bélanger, S., and Song, G.: The dynamics of absorption coefficients of CDOM and particles in the St. Lawrence estuarine system: Biogeochemical and physical implications, Mar. Chem., 128–129, 44–56, 2012.

Xu, J. L.: Shoal growth and evolution of Lingdingyang of the Pearl River mouth, Ocean Press, Beijing, China, 1985 (in Chinese).

Yamashita, Y., and Jaffé, R.: Characterizing the interactions between trace metals and dissolved organic matter using excitation-emission matrix and parallel factor analysis, Environ. Sci. Technol., 42, 7374–7379, 2008.

Yin, K., Qian, P., Chen, J., Hsieh, D. P. H., and Harrison, P. J.: Dynamics of nutrients and phytoplankton biomass in the Pearl River estuary and adjacent waters of Hong Kong during summer: preliminary evidence for phosphorus and silicon limitation, Mar. Ecol. Prog. Ser., 194, 295–305, 2000.

Zafiriou, O.C.: Sunburnt organic matter: Biogeochemistry of light-altered substrates, Limnol. Oceanogr. Bulletin, 11, 69–74, 2002.

Zepp, R. G.: Solar UVR and aquatic carbon, nitrogen, sulfur and metals cycles, in: UV effects in aquatic organisms and ecosystems, edited by: Helbling, E. W. and Zagarese, H., The Royal Society of Chemistry, Cambridge, UK, 137–183, 2003.

Zhang, S., Lu, X., Higgitt, D. L., Chen, C-T. A., Han, J., and Sun, H.: Recent changes of water discharge and sediment load in the Zhujiang (Pearl River) Basin, China, Global Planet. Change, 60, 365–380, 2008.

Zhao, H.: The Evolution of the Pearl River Estuary, Ocean Press, Beijing, China, 1990 (in Chinese).

Figure captions

Figure 1. Map of sampling stations in the Pearl River Estuary. Station names starting with letters M, W, E designate the main, west, and east transects, respectively. See Table 1 for coordinates of the stations. HM: Humen; JM: Jiaomen; HQM: Hongqimen; HeM: Hengmen; MDM: Maodaomen; HMH: Huangmaohai.

Figure 2. Excitation-emission contours of five components identified by PARAFAC modeling (left panels) and split-half validations of excitation and emission loadings (right panels). Excitation/emission maximum wavelengths are: C1: 275/320 nm; C2: <240(335)/426 nm; C3: 245/378 nm; C4: 255(370)/464 nm; C5: <240(290)/348 nm.

Figure 3. DOC concentration and a_{330} versus salinity in the PRE. Red circles denote samples collected in the low-salinity section where DOC and a_{330} showed rapid decreases or large variabilities with salinity. Blue circles denote the samples collected in the saltier zone. Solid lines in panels a and c represent means of the blue circles. Solid lines in the other panels denote linear fits of the blue circles. Dashed lines signify the 95% confidence intervals. See Table 4 for fitted equations and statistics.

Figure 4. Same as in Figure 3b,d,e–g except for FDOM components C1+C5, C2+C4, and C3.

Fiure 5. E_2/E_3 versus salinity for each cruise. Lines denote conservative mixing lines defined by the lowest- and highest-salinity points in the saltier zone.

Figure 6. Percentages of FDOM components versus salinity for each cruise. Red solid circles denote samples collected along the west transect (see Figure 1) in August.

Figure 7. BIX (a) and HIX (b) versus salinity. Red solid circles denote samples collected along the west transect (see Figure 1) in August.

Figure 8. DOC concentration versus a_{330} (a), C1+C5 (b), C2+C4 (c), and C3 (d). Solid lines denote linear fits of data for each cruise. See Table 5 for fitted equations and statistics.

Biogeosciences Discuss., https://doi.org/10.5194/bg-2018-403
Manuscript under review for journal Biogeosciences
Discussion started: 8 October 2018

Biogeosciences Discussions
Open Access
EGU

Table 1. Coordinates of sampling stations, sampling times, and water depths at the sampling stations.

Transect	Station	Lat. (°N)	Long. (°E)	Water depth (m)	Sampling date and time			
					May	August	November	January
Main transect	M01	23.033	113.517	12.0	12 (13:30)	11 (11:04)	19 (12:14)	14 (11:57)
	M02	22.967	113.540	5.5	12 (12:10)	11 (10:15)	19 (11:20)	14 (11:12)
	M03	22.790	113.623	18.6	12 (8:20)	11 (8:13)	19 (8:46)	13 (14:27)
	M04	22.710	113.682	17.9	11 (15:50)	7 (8:25)	16 (9:00)	10 (8:45)
	M05	22.585	113.691	4.9	11 (12:50)	7 (10:00)	16 (10:38)	10 (10:20)
	M06	22.523	113.751	11.4	10 (12:40)	10 (13:28)	16 (11:28)	10 (11:20)
	M07	22.426	113.752	8.8	10 (10:20)	10 (10:30)	16 (13:30)	10 (13:15)
	M08	22.257	113.722	6.9	9 (9:52)	9 (10:55)	18 (10:38)	12 (10:21)
	M09	22.122	113.715	7.7	8 (10:10)	8 (9:15)	17 (10:15)	11 (10:23)
	M10	21.994	113.722	20.4	8 (13:00)	8 (12:40)	17 (14:35)	11 (14:48)
West transect	W01	22.411	113.684	4.8	9 (14:50)	7 (12:55)	16 (14:30)	13 (10:00)
	W02	22.318	113.632	6.0	10 (8:40)	7 (14:15)	16 (15:52)	10 (15:13)
	W03	22.214	113.618	4.5	9 (8:50)	9 (9:40)	18 (9:00)	12 (9:13)
	W04	22.065	113.590	6.3	8 (15:40)	8 (14:40)	17 (16:10)	11 (9:23)
East transect	E01	22.600	113.777	8.2	11(14:40)	10 (14:42)	18 (15:28)	13 (13:30)
	E02	22.358	113.864	6.7	9 (13:05)	9 (14:35)	18 (13:10)	12 (13:26)
	E03	22.238	113.814	21.2	9 (11:25)	9 (13:00)	18 (11:35)	12 (11:59)
	E04	22.040	113.825	16.2	Not sampled	8 (10:40)	17 (11:47)	11 (11:46)

Biogeosciences Discuss., https://doi.org/10.5194/bg-2018-403
Manuscript under review for journal Biogeosciences
Discussion started: 8 October 2018

Table 2. Means (ranges) of DOC, a_{330} and intensities of fluorescent components in surface and bottom waters for each cruise. Here surf denotes surface and btm bottom.

	DOC (μmol L^{-1})	a_{330} (m^{-1})	FDOM (R.U.)		
			C1+C5	C2+C4	C3
May					
Surface	160 (110–243)	NA	NA	NA	NA
Bottom	155 (114–234)	NA	NA	NA	NA
((btm−surf)/surf)*100	−3.2	NA	NA	NA	NA
August					
Surface	117 (96–167)	1.92 (1.07–4.35)	0.90 (0.43–2.02)	0.51 (0.26–0.80)	0.30 (0.17–0.46)
Bottom	109 (78–166)	1.60 (0.56–4.27)	0.71 (0.16–1.97)	0.41 (0.11–0.87)	0.24 (0.08–0.51)
((btm−surf)/surf)*100	−6.5	−16.4	−21.0	−19.2	−18.6
November					
Surface	83 (77–133)	1.42 (0.54–3.35)	1.21 (0.47–2.30)	0.40 (0.14–0.61)	0.24 (0.10–0.37)
Bottom	82 (70–100)	1.29 (0.60–3.40)	1.10 (0.20–2.28)	0.36 (0.08–0.67)	0.21 (0.06–0.38)
((btm−surf)/surf)*100	−1.0	−8.7	−8.7	−9.8	−11.9
January					
Surface	118 (71–194)	1.34 (0.29–3.98)	1.03 (0.24–3.09)	0.30 (0.06–0.69)	0.20 (0.04–0.51)
Bottom	118 (66–207)	1.29 (0.33–4.11)	0.98 (0.23–2.95)	0.29 (0.06–0.72)	0.19 (0.04–0.53)
((btm−surf)/surf)*100	−0.1	−1.2	−5.5	−4.1	−3.6

Biogeosciences Discuss., https://doi.org/10.5194/bg-2018-403
Manuscript under review for journal Biogeosciences
Discussion started: 8 October 2018

Table 3. Means (ranges) of E_2/E_3, BIX, HIX, %(C1+C5), %(C2+C4), and %C3 in surface and bottom waters for each cruise. Here surf denotes surface and btm bottom.

	E_2/E_3	BIX	HIX	%(C1+C5)	%(C2+C4)	%C3
			August			
Surface	6.84 (4.76–8.29)	1.04 (0.95–1.14)	1.56 (1.01–2.36)	51.6 (40.2–62.2)	30.5 (23.6–39.1)	18.0 (14.2–20.7)
Bottom	6.98 (5.18–8.74)	1.07 (0.94–1.25)	1.60 (0.97–2.28)	50.2 (41.2–62.8)	31.0 (23.0–38.3)	18.8 (14.2–22.6)
((btm−surf)/surf)*100	2.0	3.4	2.4	−2.6	1.8	4.4
			November			
Surface	6.89 (5.48–9.13)	1.13 (1.02–1.30)	1.01 (0.53–1.51)	64.3 (54.2–71.1)	22.2(18.5–29.7)	13.5 (10.7–16.1)
Bottom	7.17 (6.02–8.44)	1.09 (0.68–1.30)	1.03 (0.86–1.50)	64.0 (52.4–70.3)	22.6 (18.9–31.9)	13.5 (10.4–16.5)
((btm−surf)/surf)*100	4.0	−3.8	2.5	−0.6	1.7	0.1
			January			
Surface	7.60 (6.08–11.16)	1.15 (1.04–1.53)	0.90 (0.54–1.26)	66.4 (61.6–72.2)	20.2 (15.9–23.5)	13.5 (11.7–14.9)
Bottom	7.61 (6.10–10.38)	1.16 (1.03–1.36)	0.88 (0.64–1.19)	66.3 (61.8–71.7)	20.3 (16.5–23.5)	13.4 (11.9–14.8)
((btm−surf)/surf)*100	0.2	0.5	−2.7	−0.1	0.5	−0.4

Biogeosciences Discuss., https://doi.org/10.5194/bg-2018-403
Manuscript under review for journal Biogeosciences
Discussion started: 8 October 2018

Table 4. Results of linear regression (Y = a*X + b) of DOM quantitative variables against salinity. SE denotes standard error.

	a±SE	b±SE	R^2	*p*
		DOC		
August	−1.31±0.16	121.3±2.4	0.72	<0.0001
January	−1.11±0.21	123.0±4.5	0.57	<0.0001
		a_{330}		
August	−0.042±0.006	1.97±0.09	0.67	<0.0001
November	−0.029±0.003	1.47±0.05	0.80	<0.0001
January	−0.048±0.003	1.93±0.07	0.88	<0.0001
		C1+C5		
August	−0.023±0.004	0.94±0.06	0.62	<0.0001
November	−0.035±0.005	1.43±0.10	0.67	<0.0001
January	−0.043±0.004	1.61±0.08	0.82	<0.0001
		C2+C4		
August	−0.016±0.001	0.60±0.02	0.83	<0.0001
November	−0.014±0.001	0.52±0.01	0.94	<0.0001
January	−0.014±0.001	0.53±0.02	0.90	<0.0001
		C3		
August	−0.008±0.001	0.33±0.01	0.74	<0.0001
November	−0.008±0.001	0.31±0.01	0.91	<0.0001
January	−0.008±0.001	0.32±0.01	0.86	<0.0001

Table 5. Results of linear regression (Y = a*X + b) of [DOC] against a_{330} and FDOM components. SE denotes standard error.

	a±SE	b±SE	R^2	*p*
		a_{330}		
August	22.5±1.4	72.5±2.9	0.89	<0.0001
November	18.8±2.2	61.8±3.3	0.68	<0.0001
January	32.0±2.0	71.4±3.3	0.90	<0.0001
		C1+C5		
August	43.5±2.1	76.2±2.0	0.93	<0.0001
November	16.3±1.9	66.5±2.5	0.68	<0.0001
January	40.7±2.3	72.6±3.0	0.91	<0.0001
		C2+C4		
August	100.7±11.4	64.3±5.9	0.72	<0.0001
November	52.2±9.8	65.2±4.0	0.47	<0.0001
January	159.2±13.7	66.7±4.9	0.82	<0.0001
		C3		
August	197.0±17.6	57.4±5.3	0.80	<0.0001
November	106.8±16.3	61.1±3.9	0.56	<0.0001
January	242.5±16.2	65.8±4.0	0.89	<0.0001

Table 6. Estimates for DOC and CDOM (a_{330}-based) export from the Pear River to the South China Sea based on monthly freshwater discharge rates for the sampling year and those averaged over a 10-year period from 2006 to 2016. Standard errors of the fluxes for the sampling year were derived from the standard errors of the effective [DOC] and a_{330} (Table 4), while those for the 10-year period also include the interannual variability of the freshwater discharge rate.

	Freshwater discharge ($\times 10^{10}$ m^3)		Fluxes			
			DOC ($\times 10^9$ g)		CDOM ($\times 10^9$ m^2)	
	Sampling year	10-year average	Sampling year	10-year average	Sampling year	10-year average
Spring	3.58	3.63±0.78	53.5±2.4	54.2±11.9	71.3±4.9	72.2±16.2
Summer	5.68	6.17±1.22	82.7±1.0	89.9±17.7	112±3	122±24
Autumn	5.06	2.75±0.74	49.6±2.1	27.0±7.3	74.1±1.4	40.3±10.8
Winter	3.71	1.65±0.45	54.3±1.2	24.3±6.7	71.0±1.5	31.8±8.7
Annually	18.0	14.2±1.7	240±4	195±24	329±6	266±32

Biogeosciences Discuss., https://doi.org/10.5194/bg-2018-403
Manuscript under review for journal Biogeosciences
Discussion started: 8 October 2018

Table 7. DOC concentrations and a_{330} in surface water of the Pearl River estuary reported in the literature and this study.

Month	DOC (μmol L^{-1})	Sampling Year	Reference
Jan.	71–194	2016	This study
Feb.	100–247[a]	2004	Lin (2007)
Mar.	109–266	1997	Dai et al. (2000)
	103–229[a]	2006	Lin (2007)
Apr.	84–278[b]	2007	He et al. (2010) He (2010)
May	110–243	2015	This study
	58–160[c]	2001	Callahan et al. (2004)
Jul.	109–315	1996	Dai et al. (2000)
	68–250	1999	Chen et al. (2004)
Aug.	96–167	2015	This study
	107–164[a]	2005	Lin (2007)
	94–124[b]	2008	He (2010)
Nov.	77–133	2015	This study
	82–187[c]	2002	Callahan et al. (2004)
Month	a_{330} (m^{-1})	Sampling Year	Reference
Jan.	0.29–3.98	2016	This study
May	0.37–7.48[d]	2014	Lei et al. (2018)
Jul.	1.01–3.38[d]	2013	Wang et al. (2014)
	0.54–1.98	1999	Chen et al. (2004)
Aug.	1.07–4.35	2015	This study
Nov.	0.54–3.35	2015	This study
	0.38–2.73	2002	Hong et al. (2005)

[a]Ranges were estimated using the fitted [DOC]-salinity equations in Lin (2007) over salinity 0-30.

[b]DOC concentrations upstream of Sta. M01 in the present study are excluded.

[c]Values were retrieved from figures 5a and 8b in Callahan et al. (2004).

[d]Ranges were estimated using exponential decay equations established from data in table 1 in Lei et al. (2018).

963 **Table 8.** DOC concentrations and CDOM abundances (a_{330}) in major world rivers.

River	DOM	References
DOC (μmol L^{-1})		
Amazon	235	Raymond and Bauer (2001)
	277	Cao et al. (2016)
	307 (122–492)	Seidel et al. (2016)
Mississippi	489 (231–672)	Bianchi et al. (2004)
	417[a]	Spencer et al. (2013)
Atchafalaya	331[a]	Spencer et al (2013)
St. Lawrence	307 (25–1333)	Hudon et al. (2017)
	231[a]	Spencer et al. (2013)
Mackenzie	375±100	Cooper et al. (2005)
	347 (258–475)	Raymond et al. (2007)
	402 (250–576)[b]	Osburn et al. (2009)
	363 (250–475)	Stedmon et al. (2011)
Yukon	533±242	Cooper et al. (2005)
	509 (217–1258)	Raymond et al. (2007)
	574[a]	Spencer et al. (2013)
	674 (200–1617)	Stedmon et al. (2011)
Kolyma	500±167	Cooper et al. (2005)
	594 (250–1025)	Stedmon et al. (2011)
Lena	724±283	Cooper et al. (2005)
	775 (542–1233)	Raymond et al. (2007
	948 (550–1600)	Stedmon et al. (2011)
Ob	733±167	Cooper et al. (2005)
	780 (458–1000)	Raymond et al. (2007)
	875 (375–1058)	Stedmon et al. (2011)
Yenisey	733±316	Cooper et al. (2005)
	638 (242–1050)	Raymond et al. (2007)
	754 (208–1250)	Stedmon et al. (2011)
Yellow	202 (151–280)	Wang et al. (2012)
Yangtze	169 (137–228)	Wang et al. (2012)
Pearl River	149 (72–243)[c]	This study
	a_{330} (m^{-1})	
Amazon	13.05[d]	Cao et al. (2016)
Mississippi	9.60[a]	Spencer et al. (2013)
Atchafalaya	11.55[a]	Spencer et al. (2013)
St. Lawrence	9.65[e]	Xie et al. (2012)
	2.16[a]	Spencer et al. (2013)
Mackenzie	8.30 (5.19–13.30)[b]	Osburn et al. (2009)
	6.04 (3.01–9.63)	Stedmon et al. (2011)
Yukon	17.34[a]	Spencer et al. (2013)
	14.50 (2.65–37.84)	Stedmon et al. (2011)
Kolyma	13.63 (5.77–29.19)	Stedmon et al. (2011)
Lena	26.51 (15.48–52.94)	Stedmon et al. (2011)
Ob	22.43 (6.74–30.74)	Stedmon et al. (2011)
Yenisey	22.14 (3.50–44.79)	Stedmon et al. (2011)
Yangtze (Changjiang)	2.60 (2.29–3.02)[f]	Song et al. (2017)
Pearl River	2.50 (1.04–4.35)[c]	This study

964 [a]Retrieved from DOC and CDOM fluxes and freshwater discharge rates in Spencer et al. (2013).
965 [b]From data at salinities <5
966 [c]From data at salinities <5.
967 [d]Retrieved from the spectral slope and a_{350} at Sta. 10 in Cao et al. (2016)
968 [e]Average value at Sta. SL1 and SL2 in Xie et al. (2012).
969 [f]Average value at salinities <5.

Biogeosciences Discuss., https://doi.org/10.5194/bg-2018-403
Manuscript under review for journal Biogeosciences
Discussion started: 8 October 2018

Table 9. CDOM fluxes (a_{330}-based) from major world rivers to the ocean reported in the literature. The flux estimated for the Pearl River by this study is also included for comparison.

River	Flux ($\times 10^9$ m^2 year^{-1})	Reference
Mississippi	5070	Spencer et al. (2013)
Atchafalaya	2750	Spencer et al. (2013)
St. Lawrence	490	Spencer et al. (2013)
Mackenzie	1550	Stedmon et al. (2011)
Yukon	3520	Spencer et al. (2013)
	3260	Stedmon et al. (2011)
Kolyma	1340	Stedmon et al. (2011)
Lena	17100	Stedmon et al. (2011)
Ob	7350	Stedmon et al. (2011)
Yenisey	12600	Stedmon et al. (2011)
Pearl River	266	This study

975

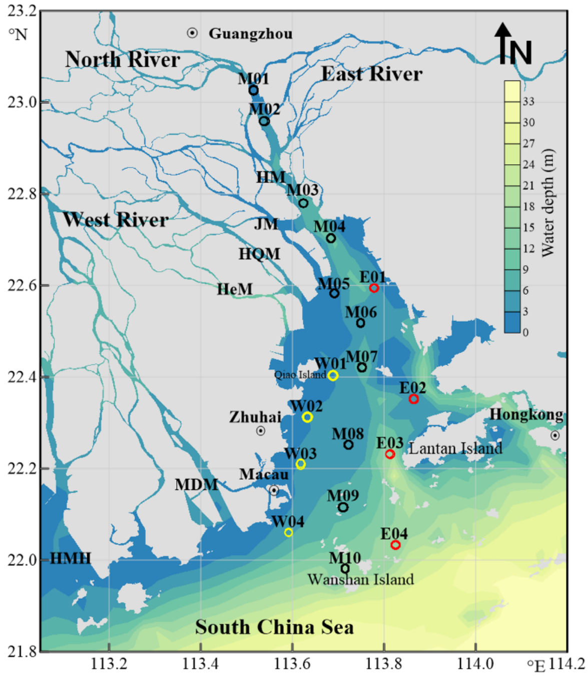

976

977 **Figure 1.** Map of sampling stations in the Pearl River Estuary. Station names starting
978 with letters M, W, E designate the main, west, and east transects, respectively. See Table
979 1 for coordinates of the stations. HM: Humen; JM: Jiaomen; HQM: Hongqimen; HeM:
980 Hengmen; MDM: Maodaomen; HMH: Huangmaohai.

981

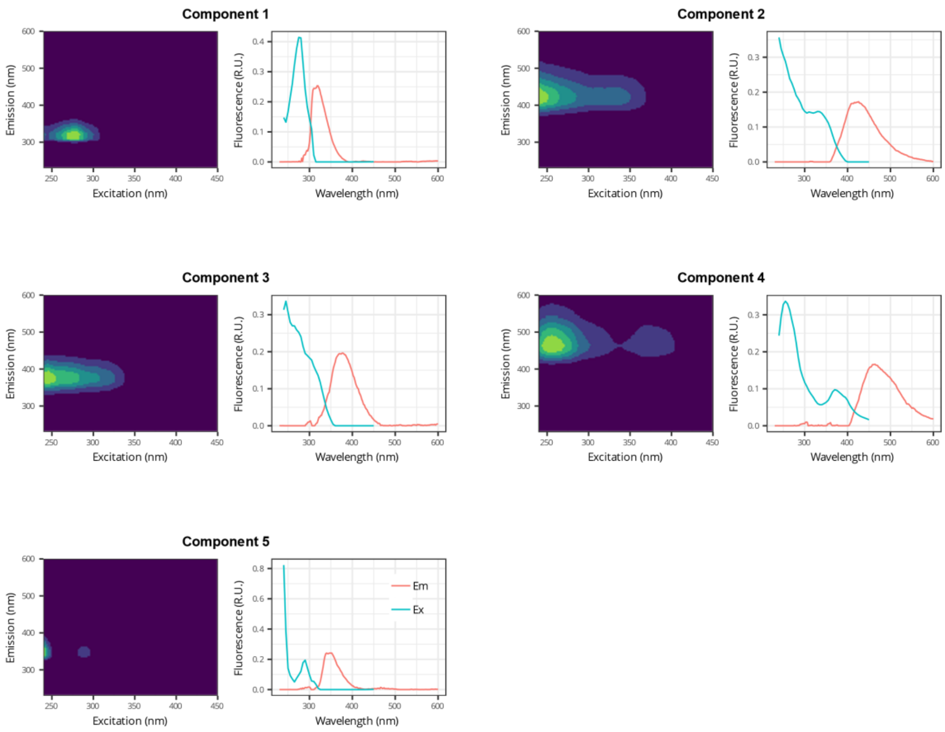

Figure 2. Excitation-emission contours of five components identified by PARAFAC modeling (left panels) and split-half validations of excitation and emission loadings (right panels). Excitation/emission maximum wavelengths are: C1: 275/320 nm; C2: <240(335)/426 nm; C3: 245/378 nm; C4: 255(370)/464 nm; C5: <240(290)/348 nm.

Biogeosciences Discuss., https://doi.org/10.5194/bg-2018-403
Manuscript under review for journal Biogeosciences
Discussion started: 8 October 2018

Biogeosciences
Discussions
Open Access

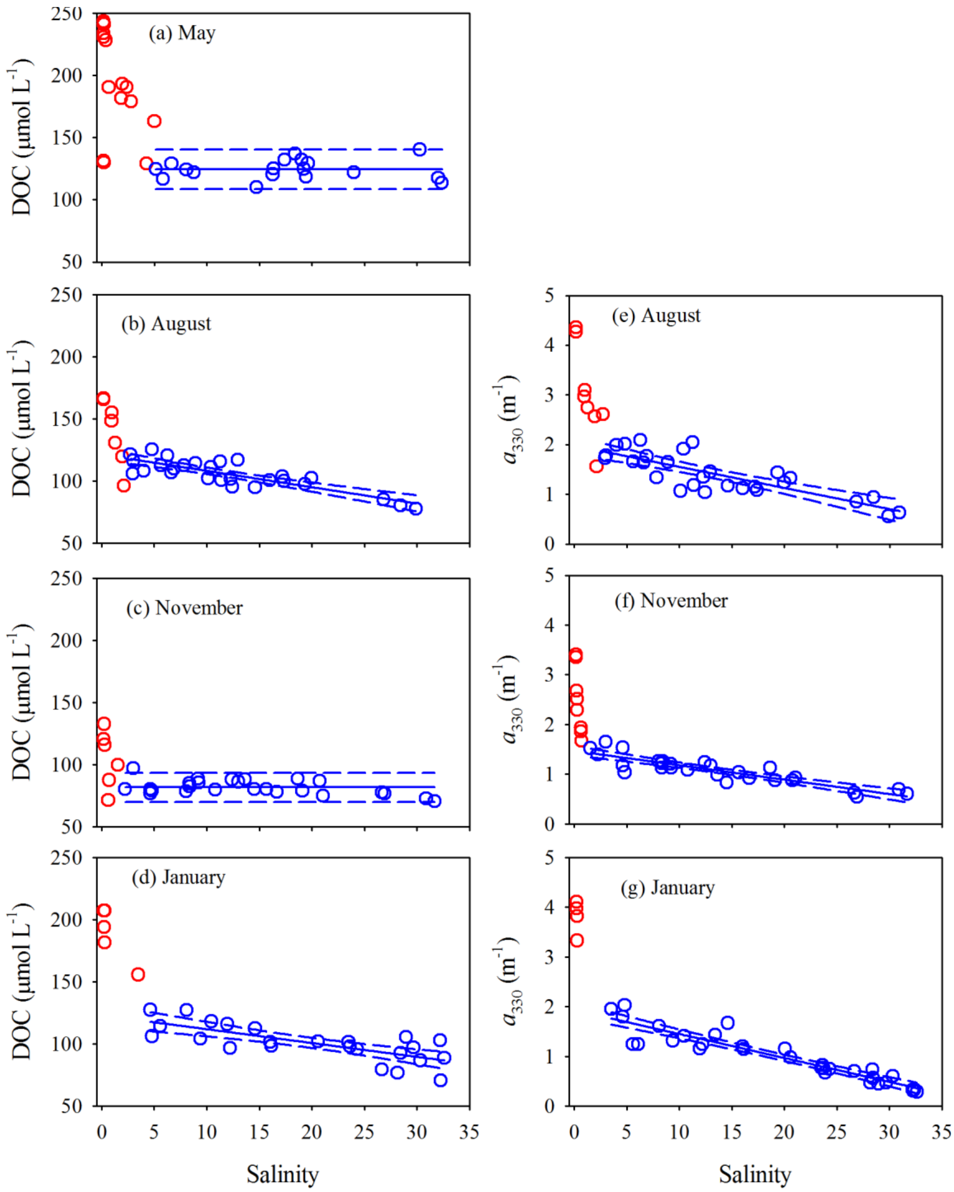

Figure 3. DOC concentration and a_{330} versus salinity in the PRE. Red circles denote samples collected in the low-salinity section where DOC and a_{330} showed rapid decreases or large variabilities with salinity. Blue circles denote the samples collected in the saltier zone. Solid lines in panels a and c represent means of the blue circles. Solid lines in the other panels denote linear fits of the blue circles. Dashed lines signify the 95% confidence intervals. See Table 4 for fitted equations and statistics.

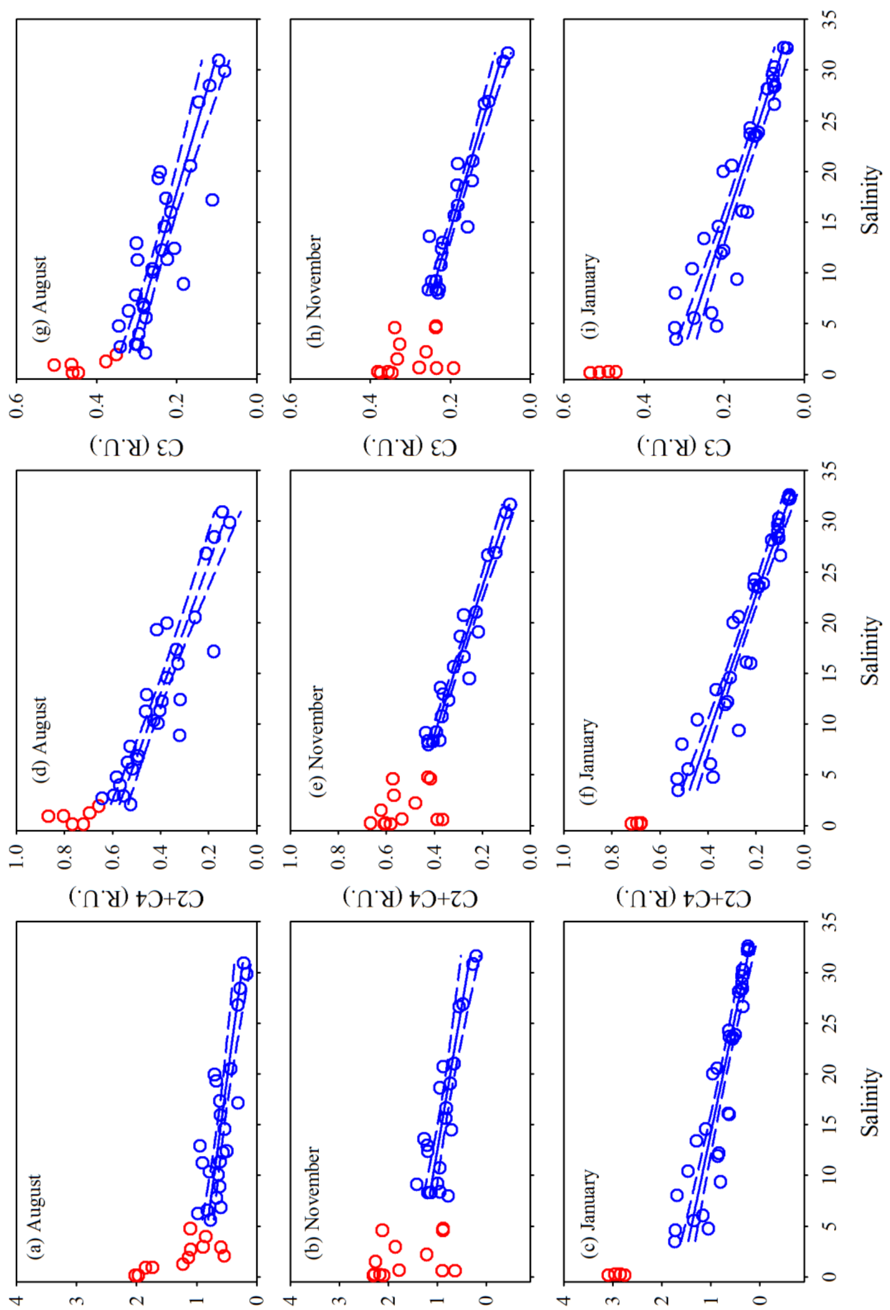

Figure 4. Same as in Figure 3b,d,e–g except for FDOM components C1+C5, C2+C4, and C3.

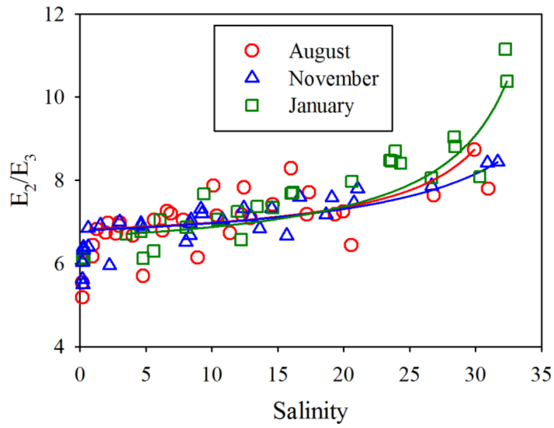

Figure 5. E_2/E_3 versus salinity for each cruise. Lines denote conservative mixing lines defined by the lowest- and highest-salinity points in the saltier zone.

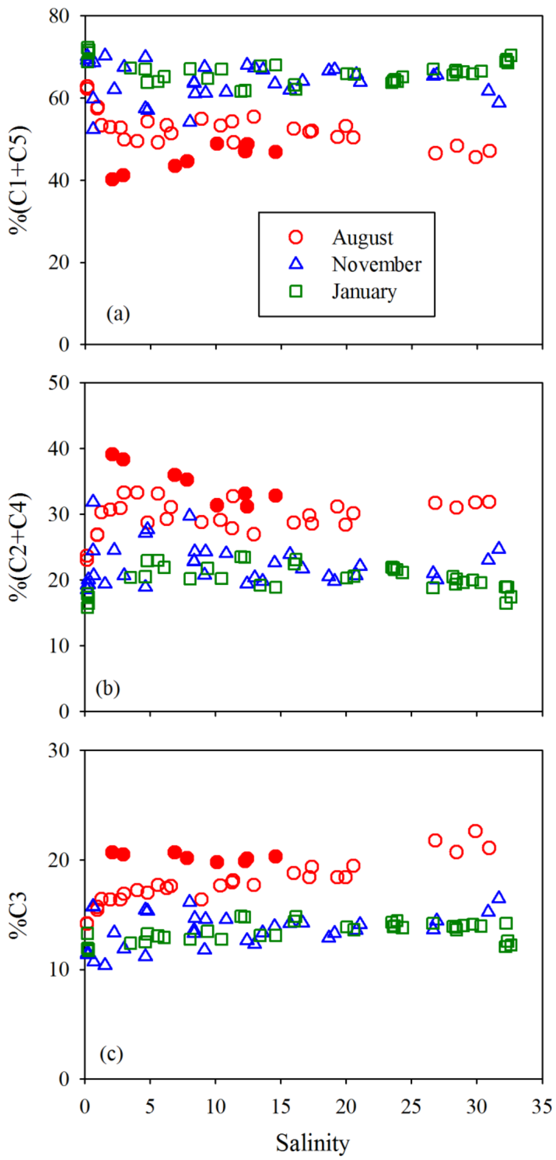

1002

1003 **Figure 6.** Percentages of FDOM components versus salinity for each cruise. Red solid circles

1004 denote samples collected along the west transect (see Figure 1) in August.

1005

Biogeosciences Discuss., https://doi.org/10.5194/bg-2018-403
Manuscript under review for journal Biogeosciences
Discussion started: 8 October 2018

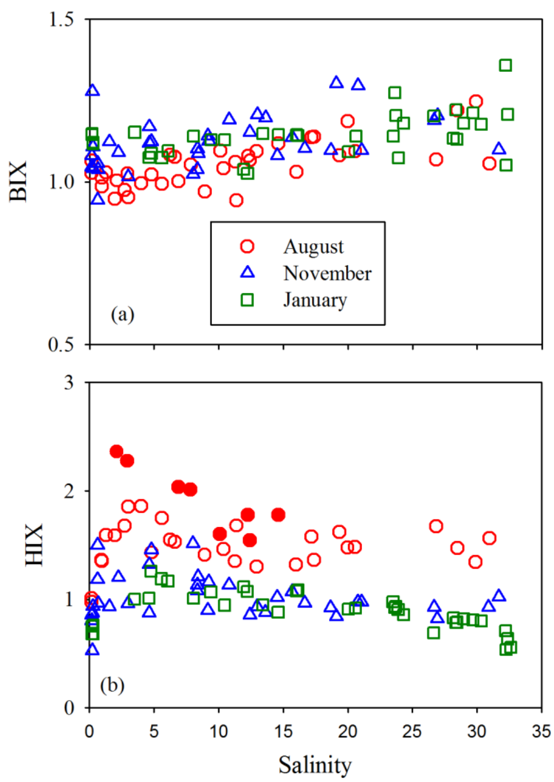

Figure 7. BIX (a) and HIX (b) versus salinity. Red solid circles denote samples collected along the west transect (see Figure 1) in August.

Biogeosciences Discuss., https://doi.org/10.5194/bg-2018-403
Manuscript under review for journal Biogeosciences
Discussion started: 8 October 2018

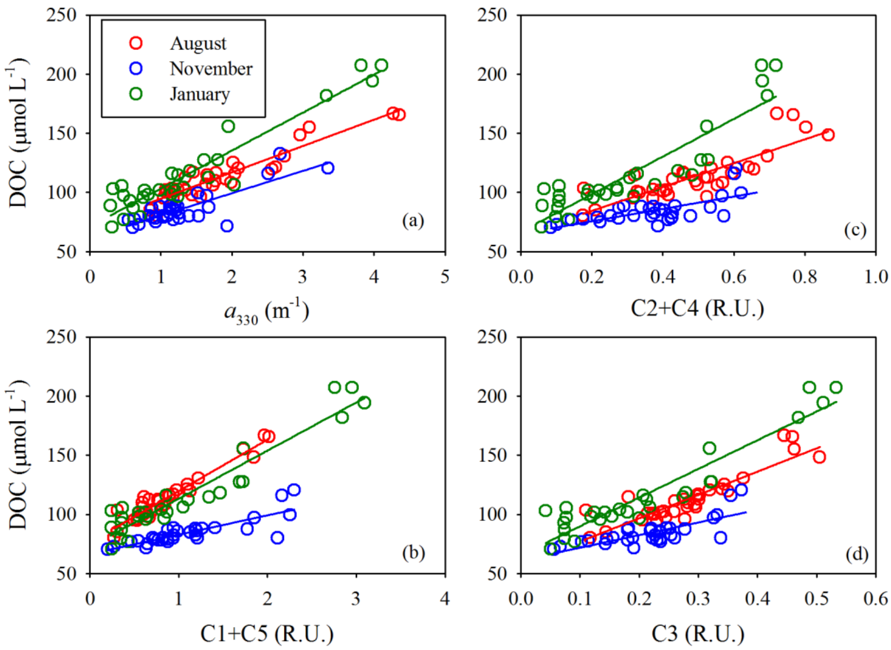

1010

1011 **Figure 8.** DOC concentration versus a_{330} (a), C1+C5 (b), C2+C4 (c), and C3 (d). Solid lines
1012 denote linear fits of data for each cruise. See Table 5 for fitted equations and statistics.